NASA TECHNICAL MEMORANDUM

NASA TM X-1924

NASA TM X-1924

FLIGHT TEST OF A 40-FOOT-NOMINAL-DIAMETER DISK-GAP-BAND PARACHUTE DEPLOYED AT A MACH NUMBER OF 3.31 AND A DYNAMIC PRESSURE OF 10.6 POUNDS PER SQUARE FOOT

by Clinton V. Eckstrom

Langley Research Center
Langley Station, Hampton, Va.

NATIONAL AERONAUTICS AND SPACE ADMINISTRATION • WASHINGTON, D. C. • FEBRUARY 1970

1. Report No. NASA TM X-1924	2. Government Accession No.	3. Recipient's Catalog No.
4. Title and Subtitle FLIGHT TEST OF A 40-FOOT-NOMINAL-DIAMETER DISK-GAP-BAND PARACHUTE DEPLOYED AT A MACH NUMBER OF 3.31 AND A DYNAMIC PRESSURE OF 10.6 POUNDS PER SQUARE FOOT		5. Report Date February 1970 6. Performing Organization Code
7. Author(s) Clinton V. Eckstrom		8. Performing Organization Report No. L-6693 10. Work Unit No. 709-12-00-01-23
9. Performing Organization Name and Address NASA Langley Research Center Hampton, Va. 23365		11. Contract or Grant No. 13. Type of Report and Period Covered Technical Memorandum
12. Sponsoring Agency Name and Address National Aeronautics and Space Administration Washington, D.C. 20546		14. Sponsoring Agency Code

15. Supplementary Notes

Technical Film Supplement L-1066 available on request

16. Abstract

A 40-foot-nominal-diameter (12.2 meter) disk-gap-band parachute was flight tested as part of the NASA supersonic high altitude parachute experiment (SHAPE) program. The test parachute (which included an experimental energy absorber in the attachment riser) was deployed from an instrumented payload by means of a deployment mortar when the payload was at a Mach number of 3.31 and a free-stream dynamic pressure of 10.6 pounds per square foot (508 newtons per square meter). The parachute deployed properly, the canopy inflating to a full-open condition at 1.03 seconds after mortar firing. The first full inflation of the canopy was immediately followed by a partial collapse with subsequent oscillations of the frontal area from about 30 to 75 percent of the full-open frontal area. After 1.07 seconds of operation, a large tear appeared in the cloth near the canopy apex. This tear was followed by two additional tears shortly thereafter. It was later determined that a section of the canopy cloth was severely weakened by the effects of aerodynamic heating. As a result of the damage to the disk area of the canopy, the parachute performance was significantly reduced; however, the parachute remained operationally intact throughout the flight test and the instrumented payload was recovered undamaged.

17. Key Words Suggested by Author(s)	18. Distribution Statement
Disk-gap-band parachutes Parachute flight tests Decelerator	Unclassified – Unlimited

19. Security Classif. (of this report)	20. Security Classif. (of this page)	21. No. of Pages	22. Price*
Unclassified	Unclassified	47	$3.00

*For sale by the Clearinghouse for Federal Scientific and Technical Information Springfield, Virginia 22151

FLIGHT TEST OF A 40-FOOT-NOMINAL-DIAMETER DISK-GAP-BAND PARACHUTE DEPLOYED AT A MACH NUMBER OF 3.31 AND A DYNAMIC PRESSURE OF 10.6 POUNDS PER SQUARE FOOT

By Clinton V. Eckstrom
Langley Research Center

SUMMARY

A 40-ft-nominal-diameter (12.2 m) disk-gap-band parachute was flight tested as part of the NASA supersonic high altitude parachute experiment (SHAPE) program. The test parachute was deployed from an instrumented payload by means of a deployment mortar when the payload was at an altitude of 168 700 ft (51.4 km), a Mach number of 3.31, and a free-stream dynamic pressure of 10.6 lb/ft^2 (508 N/m^2). The parachute deployed properly, suspension line stretch occurring 0.47 sec after mortar firing with a resulting snatch-force loading of -7.7g. The parachute canopy inflated to a full-open condition at 1.03 sec after mortar firing. For this flight test an experimental energy-absorber system was located in the payload attachment riser to limit peak loads due to the parachute opening process. The energy-absorber system was designed to limit the parachute loads to about -15g; except for the -21.2g transient peak load associated with breaking of the system restraint straps (in order to make the system operational), the maximum opening loads were limited to approximately the design level. The first full inflation of the canopy was immediately followed by a partial collapse, and the frontal area oscillated from about 30 to 75 percent of the full-open frontal area. At 1.07 sec after the first opening of the parachute, a tear occurred in the cloth near the canopy apex. This tear spread rapidly to the vent edge and the outer edge of the disk portion of the canopy. A second and third tear appeared at 2.25 and 3.26 sec after the first opening. It was later determined that the area of the canopy where these tears originated had been severely weakened by the effects of aerodynamic heating. As a result of the extensive damage which occurred to the disk area of the canopy, the parachute performance was significantly reduced. The axial-force coefficient averaged about 0.15 during the initial high deceleration part of the flight. The average effective drag coefficient was 0.41 during the descent from 146 000 ft (44.5 km) to impact (approximately 4000 ft (12 km)).

Parachute oscillation angles measured during part of the descent above 100 000 ft (30 km) ranged from 0° to $\pm 20^\circ$ with an average of about $\pm 10^\circ$. Despite the extensive damage which occurred to the canopy, the parachute remained operationally intact over the altitude interval traversed; the altitude interval extended from apogee at 253 000 ft (77 km) to ground level and the instrumented payload was recovered undamaged.

INTRODUCTION

The NASA supersonic high altitude parachute experiment (SHAPE) program is an extension of earlier efforts to provide data on parachute performance in low-density environments. (See refs. 1 and 2.) The test conditions of interest for the NASA supersonic high altitude parachute experiment program (SHAPE) were higher Mach numbers at relatively low dynamic pressures to simulate some proposed planetary entry decelerator deployment conditions.

This report presents results from the flight test of a 40-foot-nominal-diameter (12.2 meter) disk-gap-band parachute deployed at a Mach number of 3.31. Similar parachutes have previously been deployed at a Mach number of 1.91 (ref. 3) and a Mach number of 2.72 (ref. 4). The operation of the parachute deployed at a Mach number of 1.91 was highly successful and the test at a Mach number of 2.72 was also successful with the exception of canopy-shape variations and large-amplitude oscillatory parachute loads which occurred during the higher Mach number part of the flight test ($M > 1.4$). The large-amplitude oscillatory loads were later determined to have occurred primarily at the natural frequency of the parachute suspension system. (See ref. 4.) An energy-absorbing system was then developed based on preliminary work performed by Gray. (See ref. 5.) This energy absorber which was located in the payload attachment riser system was designed to limit the peak parachute opening loads and thereby reduce the effect of the oscillations of the suspension lines on the performance of the parachute canopy.

The primary purpose of the test was to make a significant increase in the deployment Mach number at the same dynamic pressure as the earlier tests and to evaluate the capability of the parachute system to withstand this more severe environment.

Motion-picture film supplement L-1066 is available on loan; a request card and a description of the film are included at the back of this paper.

SYMBOLS

a_l linear acceleration along longitudinal axis of payload, g units

$C_{A,o}$ nominal axial-force coefficient

$(C_{D,o})_{eff}$ effective drag coefficient (based on vertical descent velocity and acceleration)

D_o nominal diameter, $\left(\frac{4S_o}{\pi}\right)^{1/2}$, feet (meters)

g	acceleration due to gravity, 32.2 feet/second^2 (9.81 meters/second^2)
M	Mach number
m	mass, slugs (kilograms)
Δp	differential pressure, in. H_2O (cm H_2O)
q_∞	free-stream dynamic pressure, $\frac{1}{2}\rho_\infty V^2$, pounds/foot^2 (newtons/meter^2)
S_o	nominal surface area of parachute canopy including gap and vent, feet^2 (meters^2)
S_p	projected area of parachute canopy, feet^2 (meters^2)
t	time from vehicle lift-off, seconds
t'	time from mortar firing, seconds
V	true airspeed, feet/second (meters/second)
X,Y,Z	payload body-axis system
X_f,Y_f,Z_f	earth-fixed axis system
Z_E	local vertical axis, positive down
γ	flight-path angle measured from horizontal (positive up), degrees
δ_E	payload resultant pitch-yaw angle from local vertical, degrees
$\theta_g,\psi_g,\varphi_g$	gyro platform angles relating body-axis system to inertial coordinate system (gyro-uncaging position), degrees
$\theta_E,\psi_E,\varphi_E$	Euler angles relating body-axis system to earth-fixed axis system, degrees
ρ_∞	free-stream atmospheric density, slugs/foot^3 (kilograms/meter^3)

Dots over symbols denote differentiation with respect to time.

TEST SYSTEM

The instrumented payload was carried to the test point by an Honest John-Nike-Nike rocket vehicle. A photograph of the test vehicle in the launch position is presented as figure 1. A sketch of the test payload, shown as figure 2, locates primary components and the onboard instrumentation. The test parachute was stored in and deployed from the payload by the main mortar. The payload and test instruments have been described in reference 6. The suspended payload weight including the attachment bridle and tensiometer was 242.6 pounds (110.1 kilograms), the energy-absorber and intermediate riser weight was 6.4 pounds (2.9 kilograms), and the parachute system weight was 35 pounds (15.9 kilograms). Thus, the total descent weight of the payload-parachute system was 284 pounds (128.93 kilograms).

TEST PARACHUTE

The test parachute was a disk-gap-band (DGB) design having a nominal diameter D_o of 40 feet (12.2 meters) and a reference area S_o of 1256 square feet (116.7 square meters). Figure 3 represents the dimensional details of a gore and the general parachute-payload configuration. The test parachute was similar to those described in references 3 and 4 with the following exceptions:

(1) The test parachute described herein was not subjected to a sterilization heat cycle and therefore any dimensional changes from shrinkage such as noted in references 3 and 4 did not exist.

(2) The parachute deployment bag and mortar lid were permanently attached to the parachute canopy at eight places evenly spaced around the canopy vent edge.

(3) The parachute attachment riser system included an energy-absorber system (described in a later section) rather than the swivel used previously. (Since the payload was to have essentially no spin rate at the time of parachute deployment, it was decided to eliminate the swivel from the system for this test.)

(4) Three mechanical scratch gages (59.4 grams each) (ref. 7) were located on the upper surface of the canopy near the vent, one each on radial tapes 1, 12, and 22.

The first change was made to reduce the effect of possible material dimensional changes on parachute performance evaluation. The second change was made to eliminate the danger of damage due to intersecting trajectories of the parachute canopy and the free-flying bag and lid as reported in reference 4. The third change was made in an attempt to reduce the influence of the elasticity of the suspension lines on the aerodynamic performance of the parachute during the high deceleration period of the flight test. The

last change was made to learn more about canopy stress loads and to gain flight-test experience with the newly designed gages.

The test parachute was fabricated entirely of dacron materials with the structural members (suspension lines, radial tapes, hem tapes) being of type 52 high-tenacity dacron and the canopy cloth being regular tenacity type 55 dacron. Details concerning the fabrication of the test parachute and the parachute-payload system weight breakdown are given in tables I and II.

TABLE I.- PARACHUTE CHARACTERISTICS

Parachute type	Disk-gap-band
Nominal diameter, D_o, ft (m)	40 (12.2)
Nominal area, S_o, ft^2 (m^2)	1256 (116.7)
Number of gores and suspension lines	32
Geometric porosity, percent	12.5
Canopy cloth:	
Unit weight, oz/yd^2 (g/m^2)	2.0 (68)
Maximum elongation, percent	30 to 45
Tensile strength (ravel strip method), lb/in. (N/cm)	66 (115.5)
Permeability, $ft^3/ft^2/min$ at $\frac{1}{2}$ in. H_2O Δp ($m^3/m^2/min$ at 1.27 cm H_2O Δp)	100 to 140 (30.5 to 42.7)
Radial and hem tapes:	
Width, in. (cm)	3/4 (1.9)
Thickness, in. (cm)	0.027 (0.069)
Unit weight, oz/yd (g/m)	0.277 (7.18)
Maximum elongation, percent	28
Tensile strength, lb (N)	582 (2589)
Suspension lines:	
Unit weight, oz/yd (g/m)	0.268 (6.95)
Tensile strength, lb (N)	590 (2624)
Maximum elongation, percent	44
Riser webbing (MIL-W-25361A):	
Width, in. (cm)	$1\frac{23}{32}$ (4.37)
Thickness, in. (cm)	0.082 (0.208)
Unit weight, oz/yd (g/m)	2.29 (59.4)
Maximum elongation, percent	13
Tensile strength, lb (N)	8720 (38 788)

TABLE II.- PARACHUTE-PAYLOAD SYSTEM WEIGHT BREAKDOWN

			lb	kg
Mortar lid (measured)			0.7	0.32
Parachute deployment bag (measured)			1.1	0.50
Parachute including canopy, lines, and upper riser (measured)			33.2	15.07
	lb	kg		
Canopy cloth (estimated)	17.8	8.08		
Radial tapes (estimated)	3.3	1.50		
Hem tapes (estimated)	1.8	0.82		
Thread (estimated)	1.4	0.63		
Suspension lines (estimated)	7.3	3.31		
Upper riser (estimated)	1.6	0.73		
Energy-absorber system (measured)			5.2	2.36
Intermediate riser (measured)			1.2	0.54
Tensiometer (measured)			1.5	0.68
Bridle (measured)			1.5	0.68
Payload (measured)			239.6	108.78
Total system			284.0	128.93

DESCRIPTION OF THE ENERGY-ABSORBER SYSTEM

During the flight test of a disk-gap-band parachute deployed at a Mach number of 2.72 (ref. 4), large-amplitude variations in deceleration loads were encountered. It was later determined that these oscillatory parachute loads occurred primarily at the natural frequency of the parachute suspension system and that the amplitude was a function of the loading encountered when the parachute first opened. In an attempt to limit the maximum loads encountered during the opening process, an energy-absorber system was developed. The absorber is shown conceptually in figure 4 and was incorporated in the parachute attachment riser system shown in figure 3. A photograph of the energy-absorber system prior to use is shown in figure 5.

The primary source of energy absorption was by elongation of the polyvinyl chloride (PVC) material. The mechanism of energy absorption by this material during elongation is by heat dissipation with very little energy being stored. The force required to elongate the material is a function of the cross-sectional area and the rate at which the load is applied. The duration and amount of energy-absorbing capability of the PVC is a function of the length and the cross-sectional area of the material. The section used consisted of 53 layers of PVC film with a total thickness of 0.45 inch (1.14 cm). An

additional means of attaining energy absorption was by breaking of rows of stitches in the two parallel riser webbings. The two parallel webbings (with attached line for added strength) were intended to take up the load in the riser system when the PVC has elongated to just over three times its original length or if the PVC should break during the elongation process. During earlier tests, each row of stitching in the parallel riser webbings broke at a load of about 600 pounds (2670 newtons).

Only a limited amount of PVC could be stored in the available payload area; therefore, to prevent early dissipation of the energy-absorbing capability, retainer break straps (designed to break at a dynamic load of about 3500 pounds (15 600 newtons)) were used to prevent elongation of the PVC section during the parachute-ejection sequence through bag strip or during the early stages of the canopy inflation when the opening loads were low. The energy-absorber system was designed to be stored in the slot between the payload wall and the exterior surface of the mortar tube in such a way as to be extracted by the ejection of the parachute. Two earlier drop tests were made from aircraft to assure the structural integrity and proper deployment of the energy absorber before it was used on the rocket-launched flight test.

RESULTS AND DISCUSSION

Test Data

The flight test vehicle was launched at 9:32 a.m. mdt on October 23, 1968, at White Sands Missile Range, New Mexico. Figure 6 presents the flight sequence and the recorded times for significant flight events. Histories of altitude and relative velocity for the first 360 seconds of the flight are shown in figure 7.

Meteorological data for use in analysis of parachute test data were provided by means of an Arcas meteorological sounding rocket launch 2 hours and 28 minutes after the flight test. These data were supplemented by data from a rawinsonde which was released near the time the flight test vehicle was launched. Upper altitude winds as determined from the rocket sounding are presented in figure 8. Atmospheric density derived from measured temperature profiles is presented in figure 9.

The measured atmospheric data were used with telemetered accelerometer data and radar track data to determine histories of payload true airspeed and Mach number (fig. 10), and dynamic pressure (fig. 11) during the period immediately after initiation of parachute deployment. By definition, the initiation of parachute deployment corresponds to mortar firing ($t' = 0$). Parachute deployment was initiated at a true airspeed of 3633 feet per second (1108 meters/second) or $M = 3.31$, a dynamic pressure of 10.6 pounds per square foot (508 newtons/meter^2), and an altitude of 168 700 feet (51.4 km) above mean sea level. The altitude of the parachute-payload system during

the first 75 seconds after mortar firing, as determined by radar tracking, is presented in figure 12.

The history of force transmitted through the energy absorber and riser line as measured by the tensiometer for the first 7 seconds after mortar firing is presented in figure 13. The peak load of 1025 pounds (4559 newtons) at $t' = 0.27$ second is attributed to the full-length deployment of the parachute riser and energy absorber. The peak force of 1820 pounds (8095 newtons) at $t' = 0.47$ second was the snatch force encountered when the suspension lines were fully extended and canopy deployment began. The largest peak force of 4950 pounds (22 013 newtons) at $t' = 1.03$ seconds occurred as the parachute reached the maximum frontal area (first-full inflation) in the opening process. However, the peak force recorded at $t' = 1.03$ seconds was primarily the transient reaction load associated with breaking of the energy-absorber restraint straps. After breaking of the restraint straps, the energy absorber was allowed to become operational. As can be seen in figure 13, the opening loads were limited to the approximate 3500-pound (15 600 newtons) level for which the energy absorber was designed.

Figure 14 presents the data from three accelerometers located in the payload for the first 7 seconds after mortar firing. Positive longitudinal accelerations imposed by the firing of the mortar are not shown but were an average of 30g for a 0.02-second duration. Deceleration loads determined by use of the longitudinal accelerometer measurements are in close agreement with those recorded by the tensiometer, as would be expected. The full-length deployment of the parachute riser and energy absorber at $t' = 0.27$ second resulted in a loading of -5.7g and the snatch loading associated with suspension-line stretch at $t' = 0.47$ second was -7.7g. Except for the -21.2g transient peak load at $t' = 1.03$ seconds, associated with the breaking of the energy-absorber restraint straps, the parachute opening loads were limited to about the -15g load for which the energy absorber was designed.

Pitch and yaw motions recorded by the gyro platform during the first 7 seconds after mortar firing are shown in figure 15. Pitch angle θ_g and yaw angle ψ_g at $t' = 0$ are the direct measurements from the gyro platform referenced to the gyro offset angles introduced prior to vehicle lift-off. Offset angles were introduced into the gyro system prior to vehicle launch to counter the effects of high-altitude winds expected at flight apogee and thereby prevent the gyro platform from exceeding its yaw operating limits. Exceeding these limits would result in a loss of data for the remainder of the flight. The gyro platform offset procedure is discussed in detail in reference 8. The gyro platform pitch and yaw data presented give a real good indication of motions of the payload resulting from the varying loads imparted to the payload during the parachute deployment and inflation period and during the period of large-amplitude variations in loads transmitted to the payload through the parachute attachment system.

The flight system was not spin-stabilized and the gyro-platform-measured roll rate at mortar firing was less than 1/3 revolution per second. The roll angle of the payload as measured by the gyro platform and the roll angle of the parachute as determined from the aft camera film are presented in figure 16 for the first 7 seconds after mortar firing. The roll angle of the parachute was measured from its position at $t' = 1.0$ second when the canopy markings are first clearly visible. Initially, the parachute had little or no roll but after the canopy damage occurred, some roll was evident. The roll angle of the payload was influenced initially by the roll rate at mortar firing but with no swivel in the payload-parachute attachment system, the roll rate of the payload reversed as a result of the canopy roll in the opposite direction.

Analysis of Parachute Performance

Deployment.- The test parachute was deployed from the payload at an average ejection velocity of 113 feet per second (34.4 meters per second) based on a total suspension line plus attachment system length of 53 feet (16.2 meters) (before elongation of the energy absorber) and a measured time to line stretch of 0.47 second. As mentioned previously, the resulting snatch force was 1820 pounds (8095 newtons).

Canopy inflation.- The first inflation of the canopy occurred in a normal manner, and the projected area increased smoothly from the time of line stretch to first full opening at $t' = 1.03$ seconds as shown in figure 17. Selected frames from the aft camera film taken during the initial inflation process are shown in figure 18(a).

Immediately after the first inflation, the canopy partially collapsed as evidenced by figures 17, 18(b), and 18(c). During the sequence shown in figure 18(c), the load transmitted to the tensiometer varied considerably as indicated in the caption of each photo. The canopy load variation sequence is presented to show that the canopy projected area does not vary significantly at this time even though the tensiometer force oscillates between maximum and near-zero values. The parachute operated in the partially open condition as shown by figures 18(b) and 18(c) for just over 1 second (from $t' = 1.03$ to $t' = 2.10$ seconds) before a tear in the canopy can be seen in the frame corresponding to $t' = 2.10$ seconds as shown in figure 18(d). Additional tears in the canopy were observed on the film to have occurred at $t' = 3.28$ and $t' = 4.29$ seconds as also shown in figure 18(d). The parachute canopy did not again attain full inflation during the 60 seconds of film coverage. The partial canopy collapse after the first full inflation was expected based on results of previous flight tests for disk-gap-band parachutes. (See refs. 3, 4, and 9.) It was anticipated, however, that use of the energy absorber in the riser system would limit the opening load and the effects of suspension-line elasticity and, as a result, possibly reduce the severity of the canopy collapse and subsequent shape variations. The opening load was limited and for the 1 second of useful data available for comparison, it

does appear that the canopy collapse was less severe for the first second of operation on this test when compared with the flight test from reference 4 as shown in table III:

TABLE III.- COMPARISON OF FLIGHT TESTS

Deployment Mach number	Deployment dynamic pressure, psf	Time of first full inflation, t', sec	Minimum area ratio experienced, $S_p/S_{p,final}$	Average area ratio for 1 sec time from first inflation $(S_p/S_{p,final})_{av}$	Data source
3.31	10.6	1.03	0.42	0.57	Figure 17
2.72	9.7	.96	.21	.47	Reference 4

Because the tests compared were initiated at different Mach numbers, the improved performance cannot positively be attributed directly to the energy absorber. There also is no assurance that the same results would be achieved if each of the tests were to be repeated because the opening of a flexible parachute canopy is not an identically repeatable process.

Drag efficiency.- The axial-force coefficient $C_{A,o}$ is presented in figure 19 as a function of time from mortar deployment. In the time interval from $t' = 0.8$ to $t' = 3.0$ seconds, the axial-force coefficient was determined from accelerometer data in 0.01-second increments based on the following equation:

$$C_{A,o} = - \frac{m_{total} g a_l}{q_\infty S_o}$$

In the time interval from $t' = 3.0$ to $t' = 7.0$ seconds, the axial-force coefficient was determined from accelerometer data averaged over 0.1-second time intervals also by using the preceding equation. During the 1-second time interval, prior to the time damage was observed for the parachute canopy, the average axial-force coefficient was 0.24. After the first canopy damage occurred, the average axial-force coefficient was lower, and averaged 0.15 from $t' = 3.0$ to $t' = 7.0$ seconds. Payload drag was small compared with parachute drag and was neglected in the calculations.

As an additional check of the average axial-force coefficient of the system, a point-mass computer simulation indicated that an axial-force coefficient from 0.1 to 0.2 would approximate the experienced flight velocity and altitude profiles that were shown in figures 10 and 12.

After apogee and during the early descent portion of the flight test, the payload-parachute system achieved velocities as great as 1610 feet per second (490 meters per

second) as was shown in figure 7. The axial-force coefficient was determined during this time interval in 1-second increments over a Mach number range from 0.63 to 1.53. The resulting values are presented in figure 20. The equation used in determining the axial-force coefficient during this interval was as follows:

$$C_{A,o} = \frac{m_{total}}{q_\infty S_o}(\dot{V} + g \sin \gamma)$$

where the system velocity and velocity differential were obtained from radar data. Again, the payload drag was small in comparison with the parachute drag and was neglected in the calculations.

At the higher Mach numbers, the lower values of $C_{A,o}$ are probably indications of a partially inflated and fluctuating canopy shape. At the lower Mach numbers, the damaged canopy was able to maintain a larger drag area as indicated by the effective drag coefficient discussed in the following paragraph. The average axial-force coefficient during the interval shown was 0.36.

The variation of the vertical descent velocity and the effective drag coefficient are presented in figure 21. The values of effective drag coefficient are based on vertical descent velocity, acceleration, and the system mass as shown by the following equation:

$$(C_{D,o})_{eff} = \frac{2m_{total}}{\rho_\infty \dot{Z}_E^2 S_o}(g - \ddot{Z}_E)$$

During the descent portion of the flight test, the average effective drag coefficient $(C_{D,o})_{eff}$ was about 0.41. This value is about 23 percent less than that of a similar but undamaged DGB parachute tested and discussed in reference 3.

Stability.- The payload pitch and yaw motions and the payload roll rate immediately after parachute deployment were discussed earlier with data presented in figures 15 and 16. During the descent portion of the flight test from an altitude 137 000 feet (42 km) down to an altitude of 100 000 feet (30 km), the gyro platform data was transformed to the earth-fixed Euler angle system shown in figure 22. The data transformation method is presented in reference 8. Although the aft camera film did not cover this data period, results from a previous flight test (ref. 3) leads to the expectation that the data shown in figure 23 should represent the attitude history of the payload and parachute acting together like a rigid body and should therefore be a direct indication of the stability of the damaged parachute system.

Parachute damage.- The extent of damage sustained by the parachute immediately after deployment was shown previously in figure 18. A postflight inspection of the recovered parachute located the specific damaged area shown in figure 24. It appears that further damage beyond that seen in figure 18 did not occur. The major damage was

sustained by the disk area of gores 8, 12, and 22. The postflight examination also revealed that the parachute material had stiffened in an area around the canopy vent as shown in figure 25. It is believed that this area of stiffened material resulted when the canopy cloth cooled after it was exposed to aerodynamic heating; this heating occurred after parachute deployment during the high Mach number part of the flight test. Although it was known prior to flight that aerodynamic heating could be a problem, one of the test objectives was to determine whether the exposure would be detrimental since the parachute was subjected to the high rate of heat input for a very short period of time. On a previous deployment at a Mach number of 2.72 (ref. 4), no evidence of aerodynamic heating was found. A comparison of stagnation temperatures as a function of time for this flight test starting at a Mach number of 3.31 and of the previous flight test at a deployment Mach number of 2.72 showed that the heating environment was much more severe for this flight test.

As mentioned earlier, there were three mechanical scratch gages, which recorded maximum loads only, located near the canopy vent on radial tapes 1, 12, and 22. It was at these points that two of the three areas of damage started. Although the mass of each gage was only 54.5 grams, the additional loads imposed by these point masses were probably sufficient to fail the canopy cloth which had been severely weakened by the aerodynamic heating. The load values recorded by the mechanical gages were 172 pounds (765 newtons) at radial tape numbers 1 and 22, and 122 pounds (543 newtons) at radial tape number 12. This value is an average of 155 pounds (689 newtons) which when multiplied by the total number of radial tapes (32) gives a total load of 4960 pounds (22 063 newtons) and is close to the maximum total load recorded by the tensiometer in the attachment riser system.

CONCLUSIONS

The 40-foot-nominal-diameter (12.2 meters) disk-gap-band test parachute was deployed from an instrumented payload by means of a deployment mortar when the payload was at a Mach number of 3.31, and a free-stream dynamic pressure of 10.6 pounds per foot^2 (508 newtons per meter^2). Based on an analysis of the data, it is concluded that:

1. The mortar properly ejected the parachute system from the payload.

2. The parachute canopy inflation process began immediately, the first inflation occurring at 1.03 seconds. The parachute canopy then assumed a varying partially inflated shape. At 2.10 seconds and again at 3.28 and 4.29 seconds, the canopy was severely damaged by tears which occurred in the disk portion of gores 8, 12, and 22.

The canopy did not attain a steady fully inflated shape during the 60 seconds of aft-camera film coverage.

3. Inclusion of the energy absorber in the riser system resulted in limiting the parachute opening loads to about the -15g design level except for the -21.2g transient peak load associated with breaking of the restraint straps which allowed the energy-absorber system to become operational.

4. The energy-absorber in the riser system was at least partially successful in reducing the large-amplitude variations in loads believed to be principally a result of an oscillation set up by the elastic suspension lines of the parachute system.

5. For the first second of parachute operation (during which the canopy was undamaged), the nominal axial-force coefficient averaged about 0.24. After the first canopy damage occurred, the average axial-force coefficient was lower, and averaged 0.15 during the initial deceleration part of the flight test. During the high-velocity-descent part of the flight test, the axial-force coefficient averaged 0.36. The effective drag coefficient averaged 0.41 during the equilibrium-descent part of the flight test.

6. The canopy sustained extensive damage in the disk area beginning about 1 second after the first full inflation of the parachute. This damage is attributed primarily to aerodynamic heating which severely weakened the canopy material. This condition was undoubtedly aggravated by the fact that three mechanical scratch gages were located in the canopy area near where the aerodynamic heating problem was most severe.

Langley Research Center,
National Aeronautics and Space Administration,
Langley Station, Hampton, Va., November 6, 1969.

REFERENCES

1. McFall, John C., Jr.; and Murrow, Harold N.: Parachute Testing at Altitudes Between 30 and 90 Kilometers. J. Spacecraft Rockets (Eng. Notes), vol. 4, no. 6, June 1967, pp. 796-798.

2. Murrow, Harold N.; and McFall, John C., Jr.: Summary of Experimental Results Obtained From the NASA Planetary Entry Parachute Program. AIAA Paper No. 68-934, Sept. 1968.

3. Preisser, John S.; and Eckstrom, Clinton V.: Flight Test of a 40-Foot-Nominal-Diameter Disk-Gap-Band Parachute Deployed at a Mach Number of 1.91 and a Dynamic Pressure of 11.6 Pounds Per Square Foot. NASA TM X-1575, 1968.

4. Eckstrom, Clinton V.; and Preisser, John S.: Flight Test of a 40-Foot-Nominal-Diameter Disk-Gap-Band Parachute Deployed at a Mach Number of 2.72 and a Dynamic Pressure of 9.7 Pounds Per Square Foot. NASA TM X-1623, 1968.

5. Gray, J. Harvey: Attenuation of Deployment and Opening Forces of Certain Aerodynamic Decelerators. Proceedings – Symposium on Parachute Technology and Evaluation, Vol. II, Earl C. Myers, ed., FTC-TDR-64-12, U.S. Air Force, 1964, pp. 502-508.

6. Preisser, John S.; Eckstrom, Clinton V.; and Murrow, Harold N.: Flight Test of a 31.2-Foot-Diameter Modified Ringsail Parachute Deployed at a Mach Number of 1.39 and a Dynamic Pressure of 11.0 Pounds Per Square Foot. NASA TM X-1414, 1967.

7. Hoffman, Ira S.: Evaluation of a Parachute-Load-Distribution Measuring System During Low-Altitude Drop Tests. NASA TM X-1832, 1969.

8. Preisser, John S.; and Eckstrom, Clinton V.: Flight Test of a 30-Foot-Nominal-Diameter Cross Parachute Deployed at a Mach Number of 1.57 and a Dynamic Pressure of 9.7 Pounds Per Square Foot. NASA TM X-1542, 1968.

9. Bendura, Richard J.; Huckins, Earle K., III; and Coltrane, Lucille C.: Performance of a 19.7-Meter-Diameter Disk-Gap-Band Parachute in a Simulated Martian Environment. NASA TM X-1499, 1968.

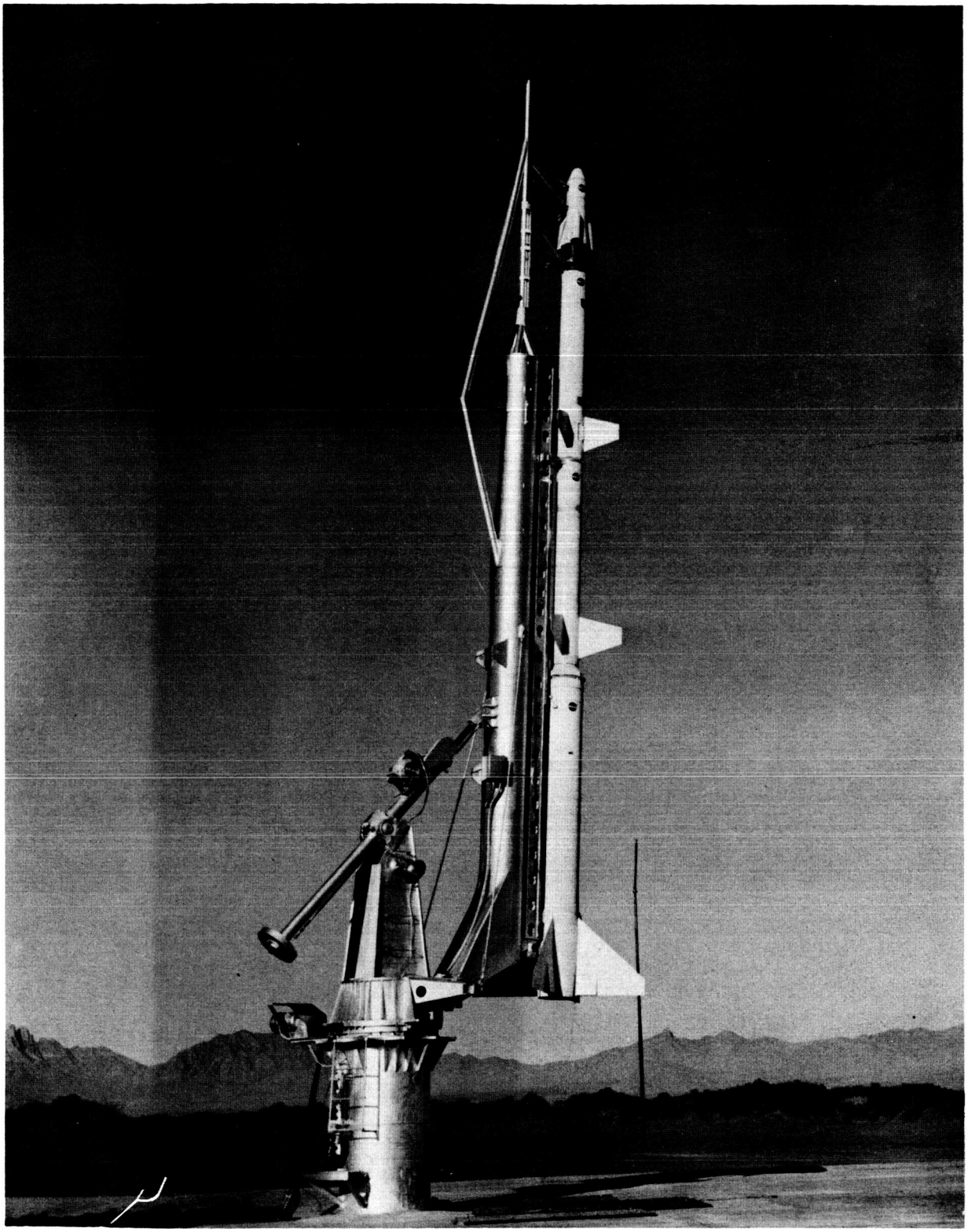

Figure 1.- Photograph of vehicle configuration. U.S. Army photograph. L-69-5114

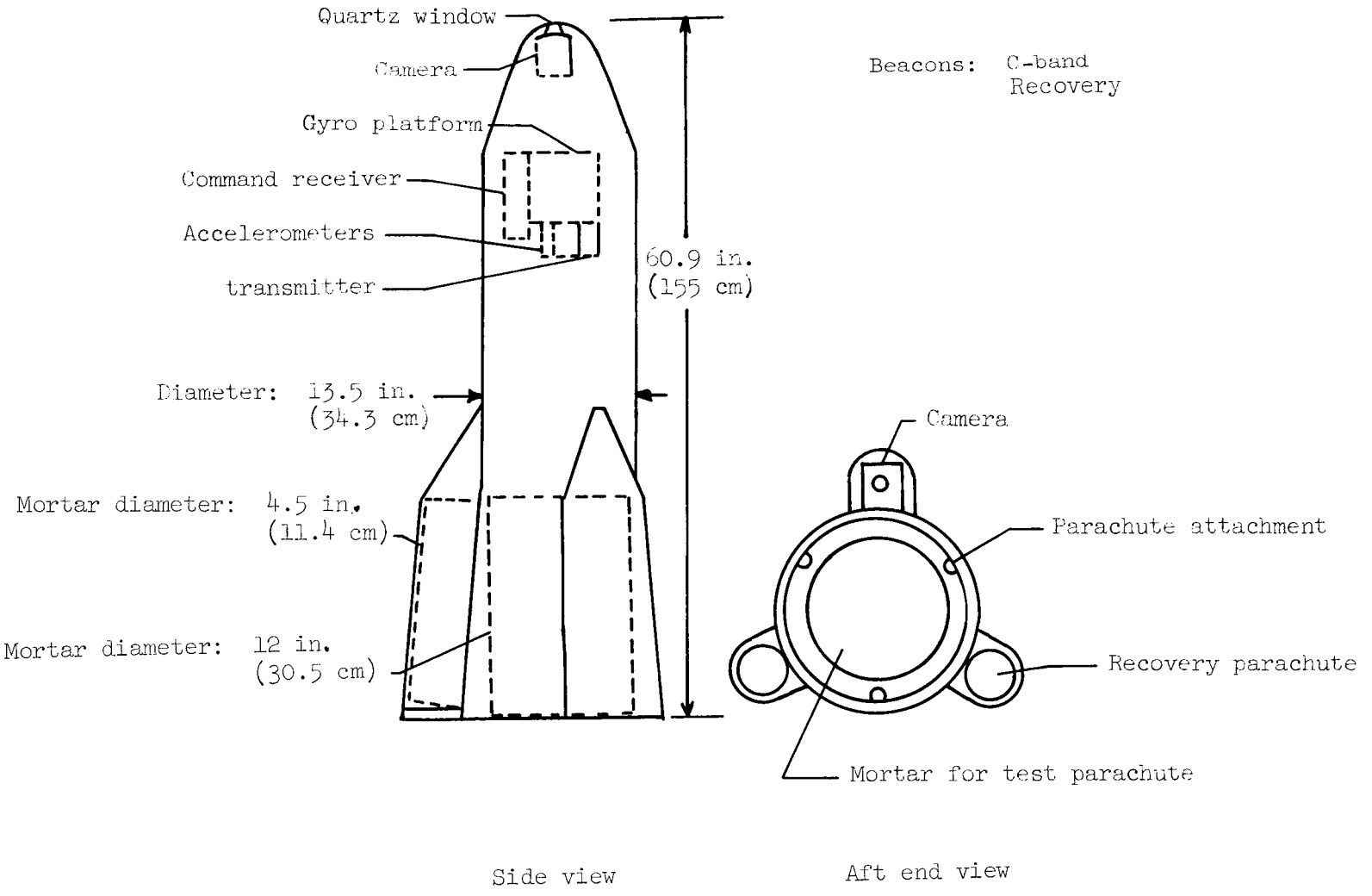

Figure 2.- Test payload.

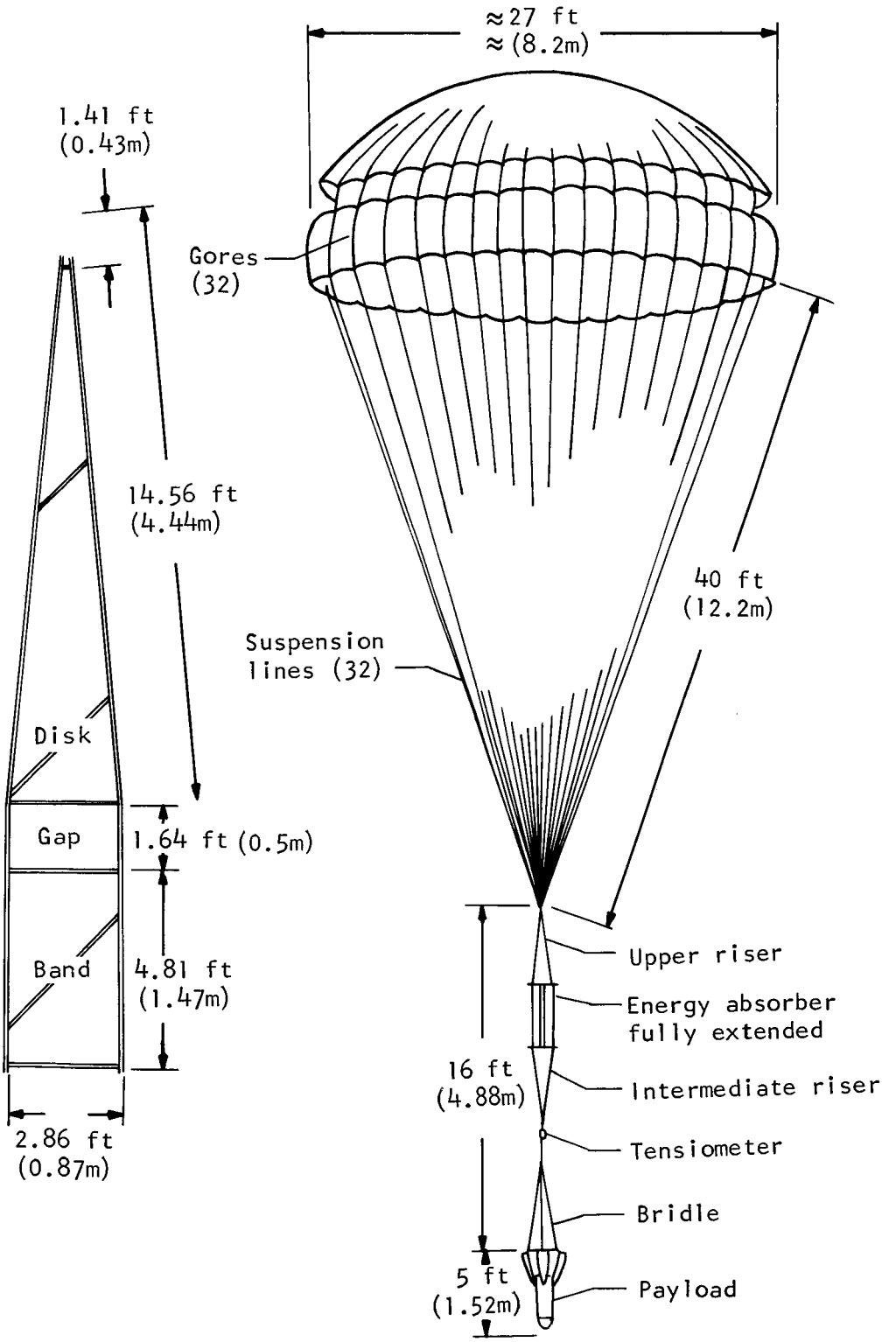

Figure 3.- Parachute-gore dimensional details and flight configuration.

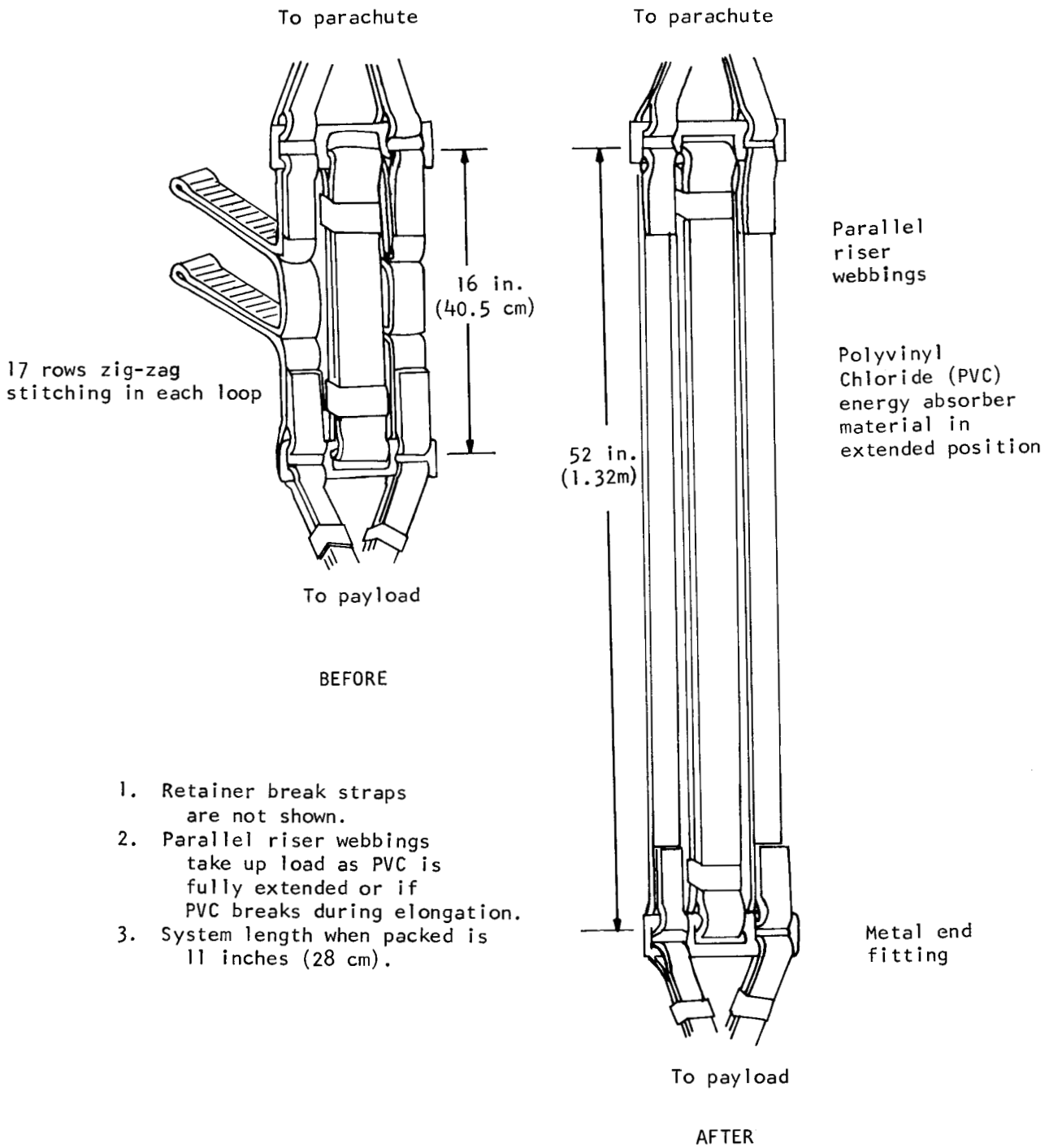

Figure 4.- Conceptual design of energy absorber.

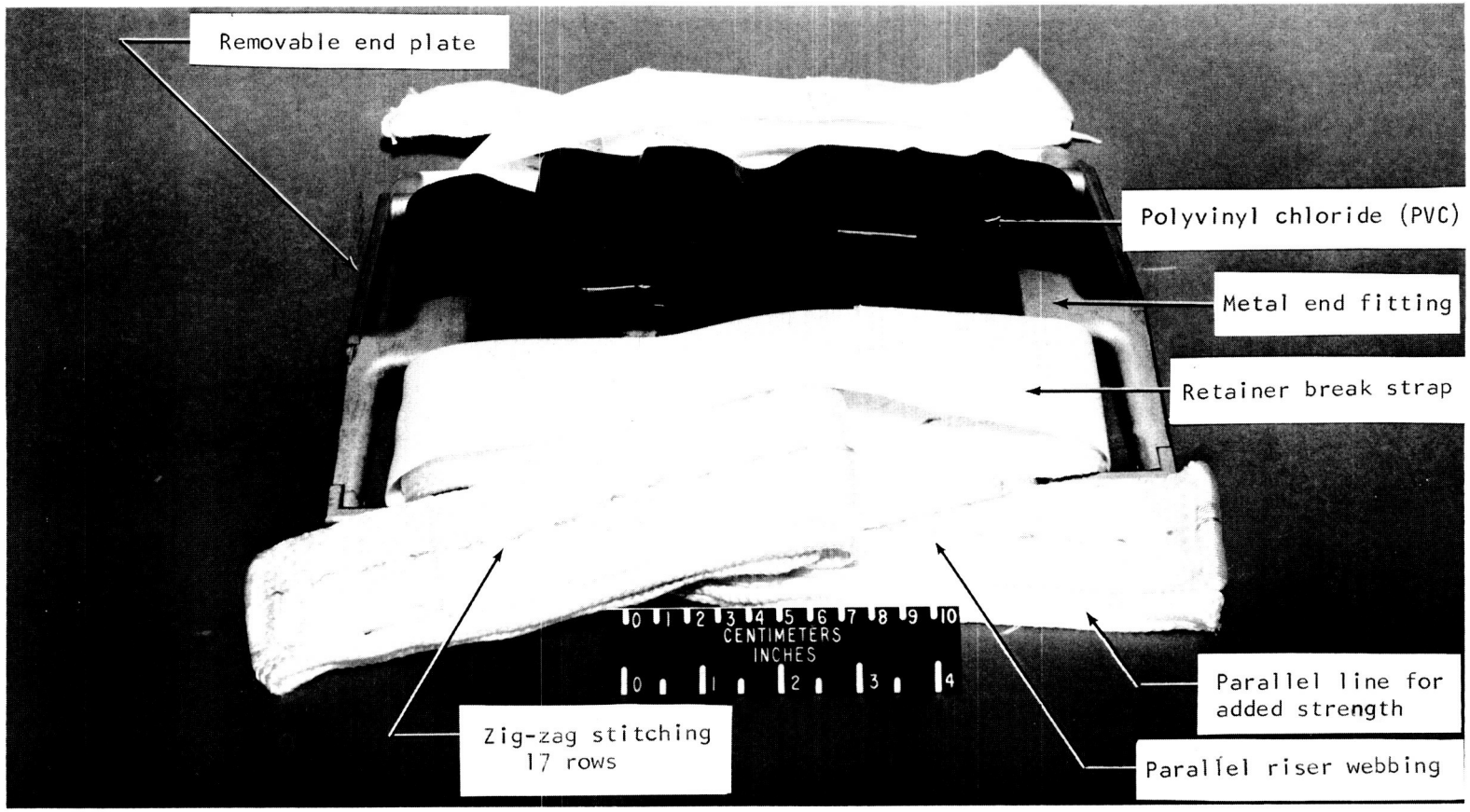

Figure 5.- Energy-absorber system.

L-69-6319

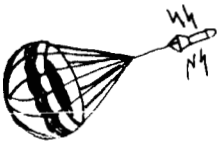

7. Maximum opening load

6. Mortar ejection of parachute

5. Radio command

4. Payload separation

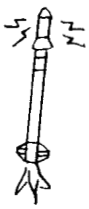

3. Third-stage ignition

Event	Time, t, sec
1	0
2	10.05
3	28.66
4	43.15
5	59.45
6	60.20
7	61.25
8	2400.0

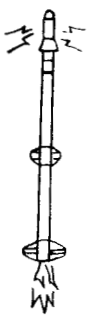

2. Second-stage ignition

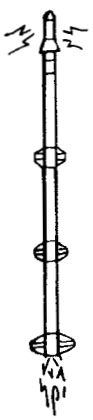

1. Vehicle lift-off

8. Impact

Figure 6.- Flight sequence of events.

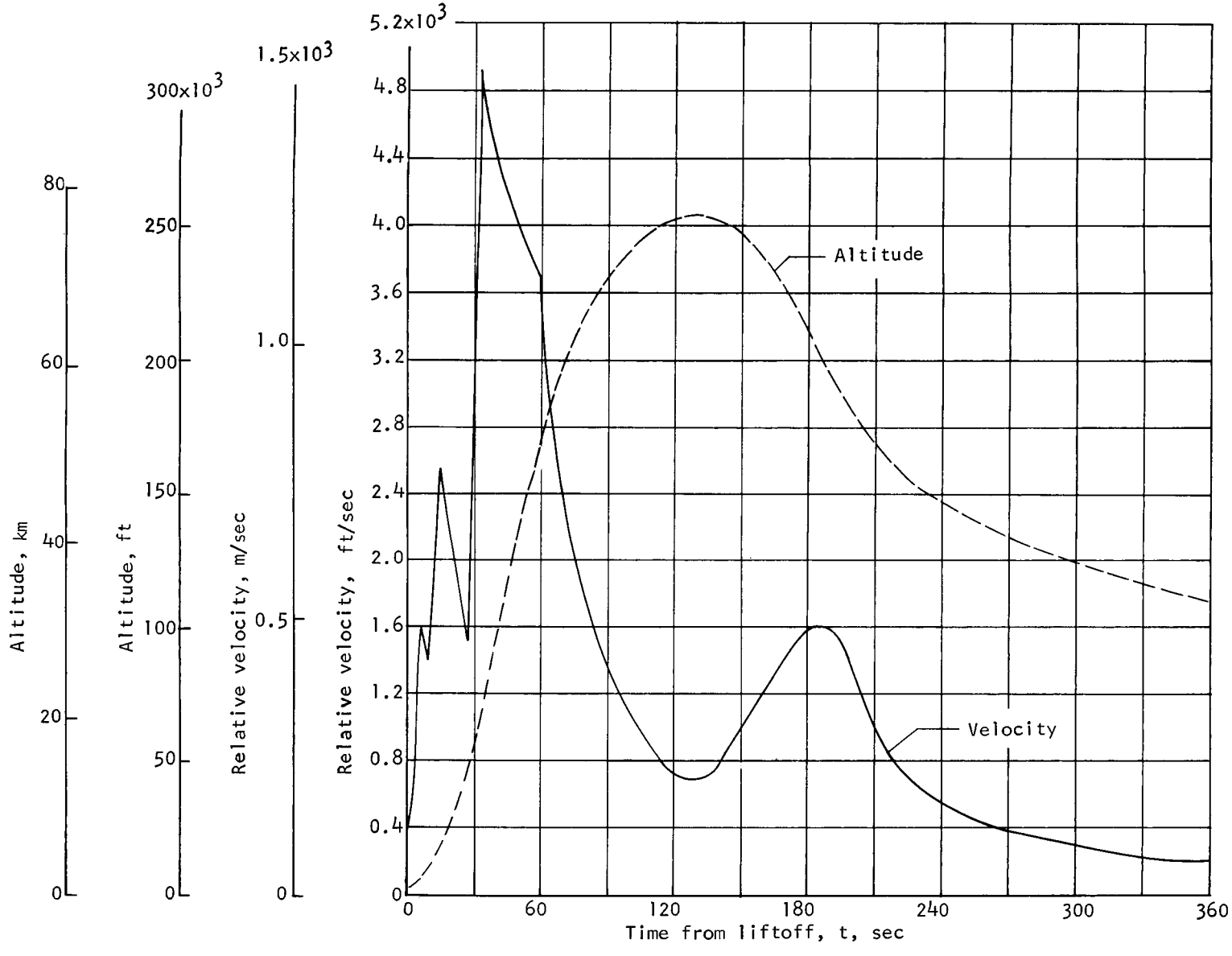

Figure 7.- Time histories of altitude and relative velocity.

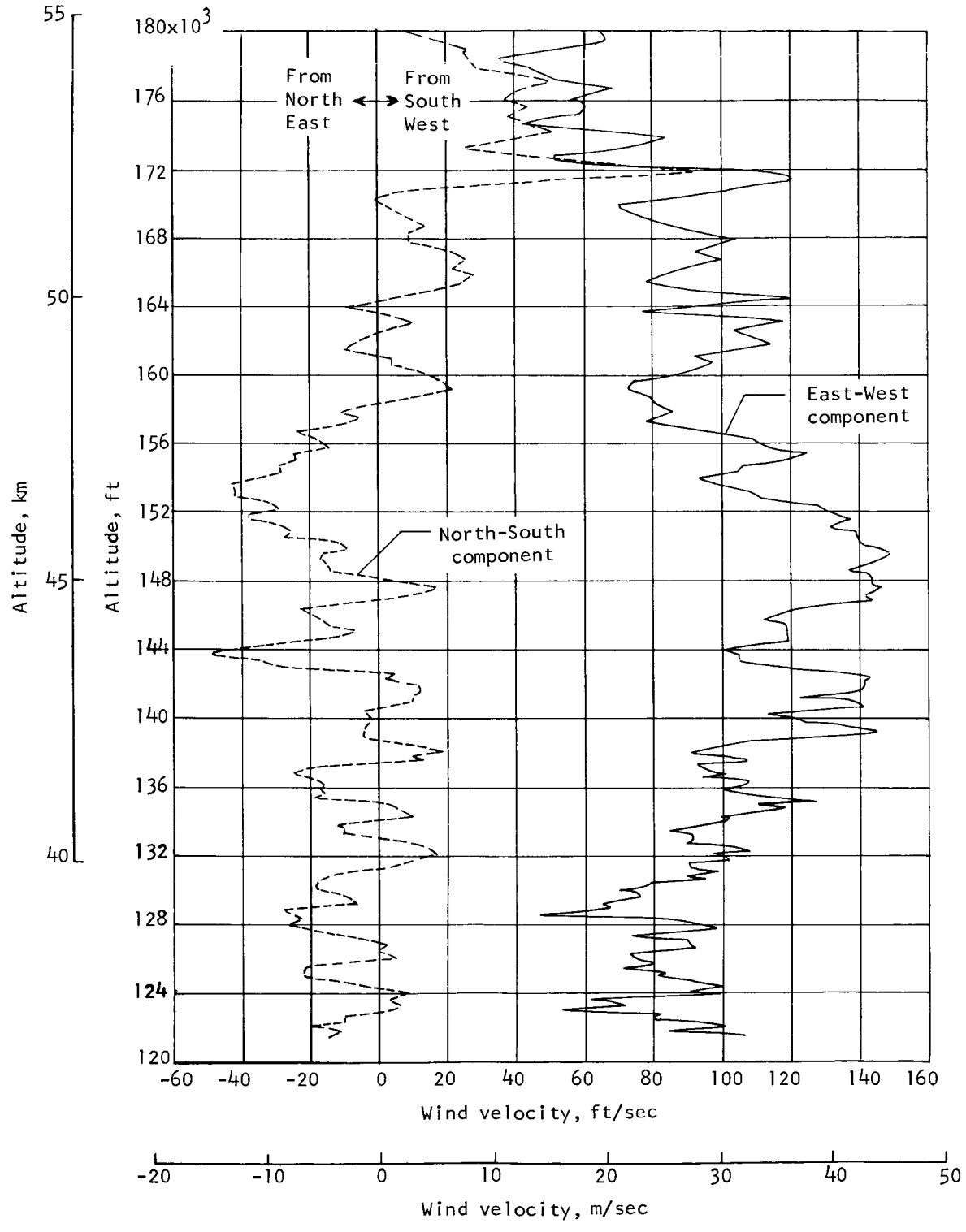

Figure 8.- Wind-velocity profile in north-south and east-west components.

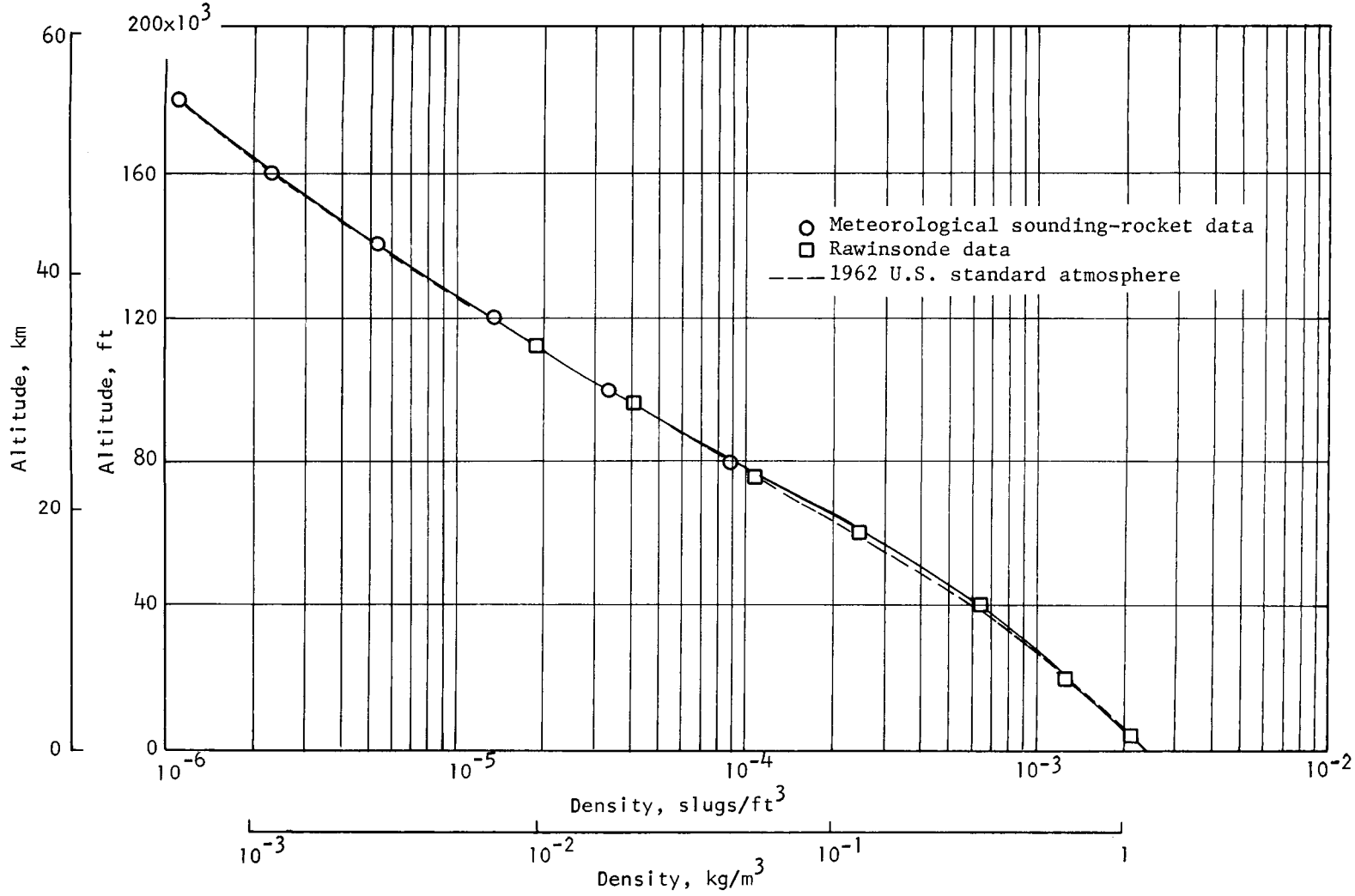

Figure 9.- Atmospheric density profile.

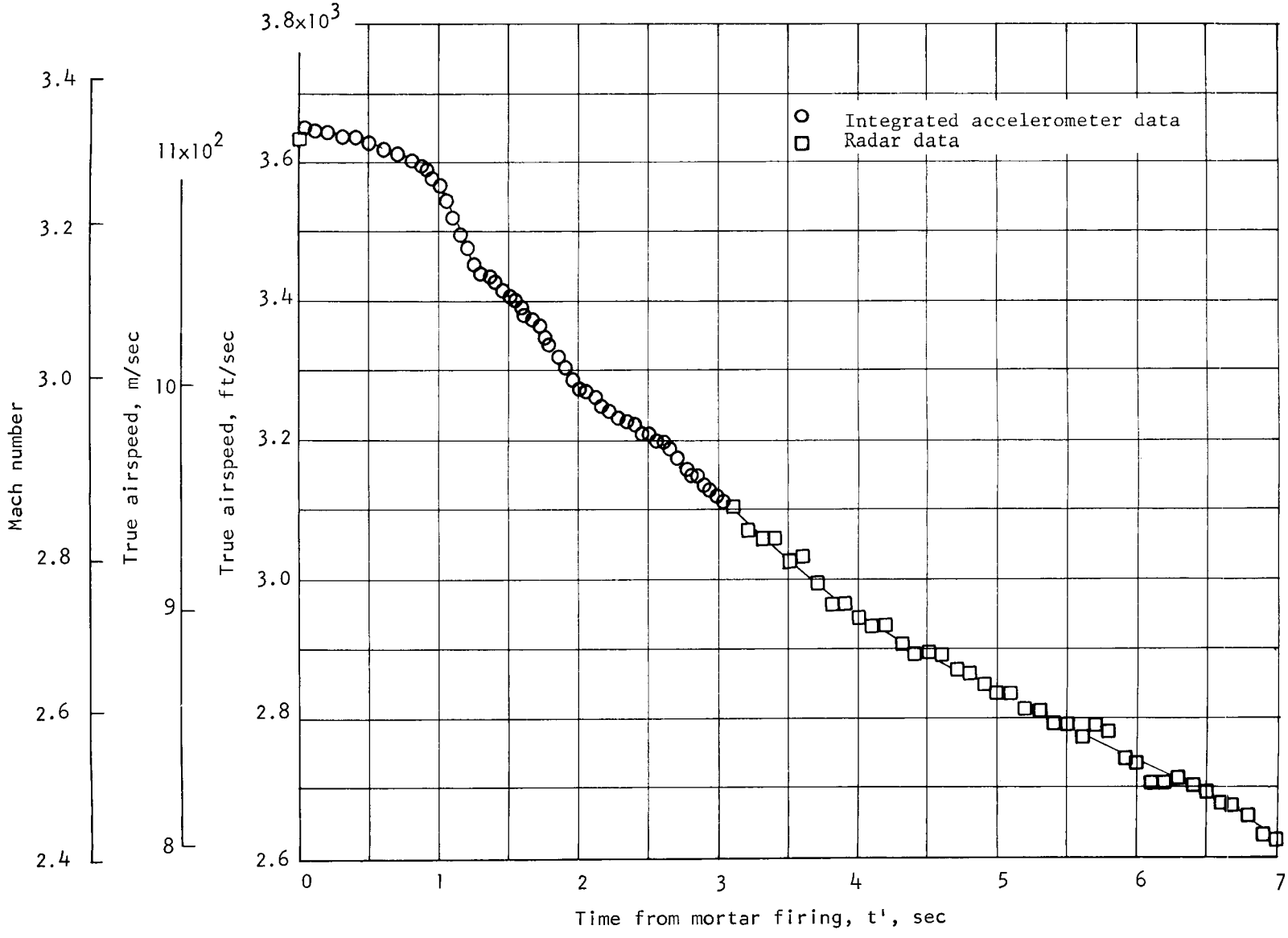

Figure 10.- Mach number and true airspeed time histories after mortar firing.

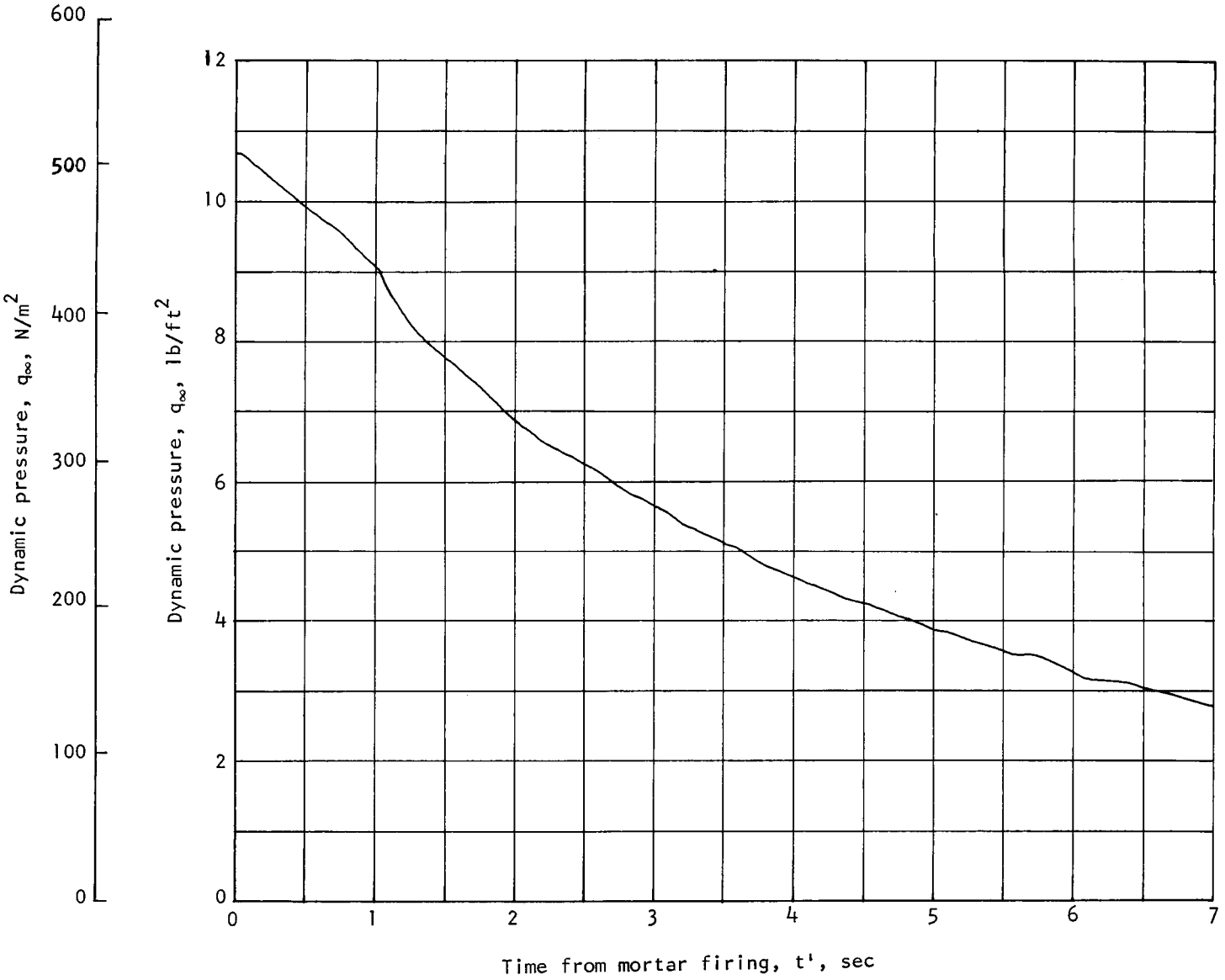

Figure 11.- Dynamic-pressure time history after mortar firing.

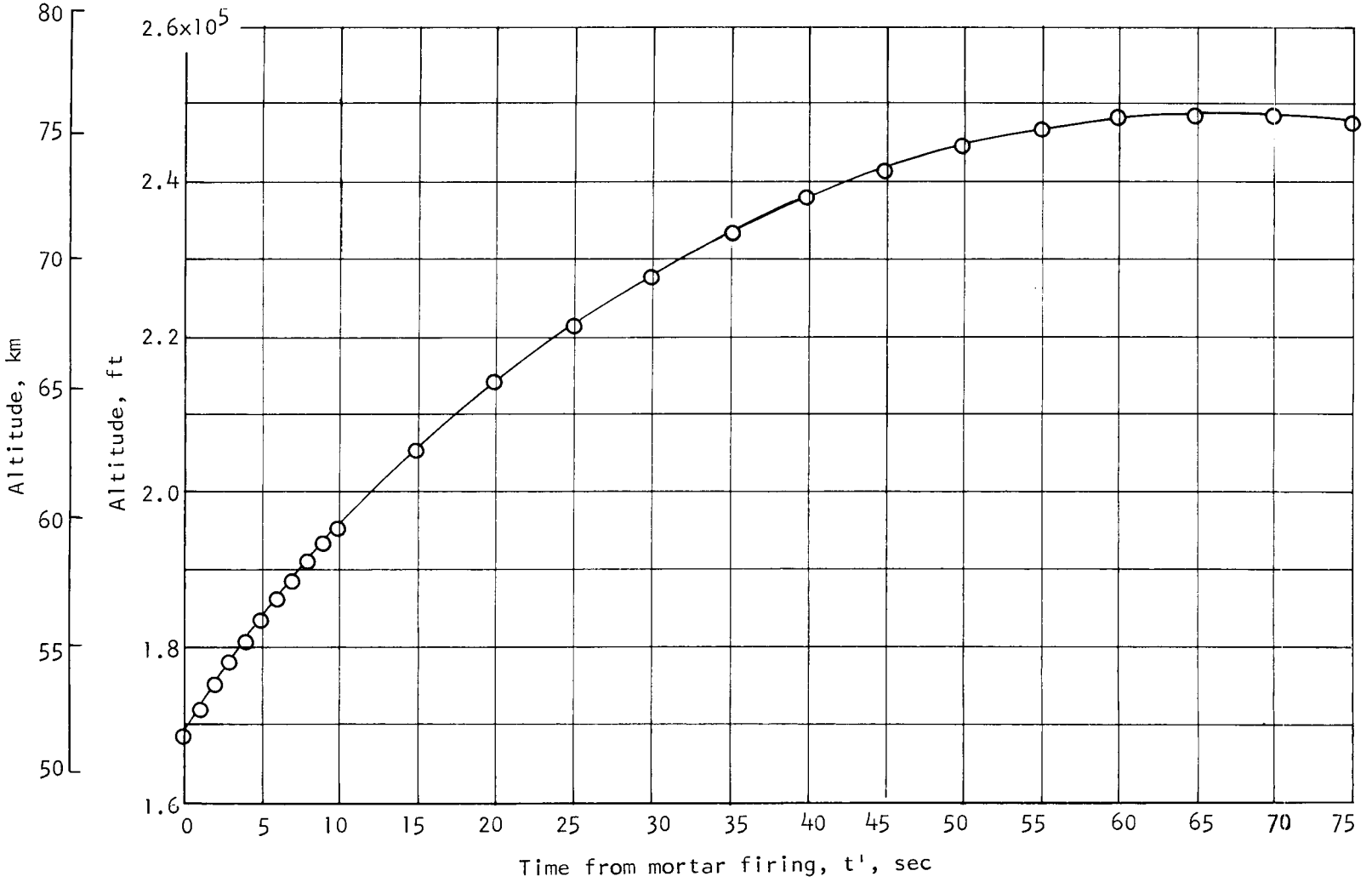

Figure 12.- Altitude time history for the first 75 seconds after mortar firing.

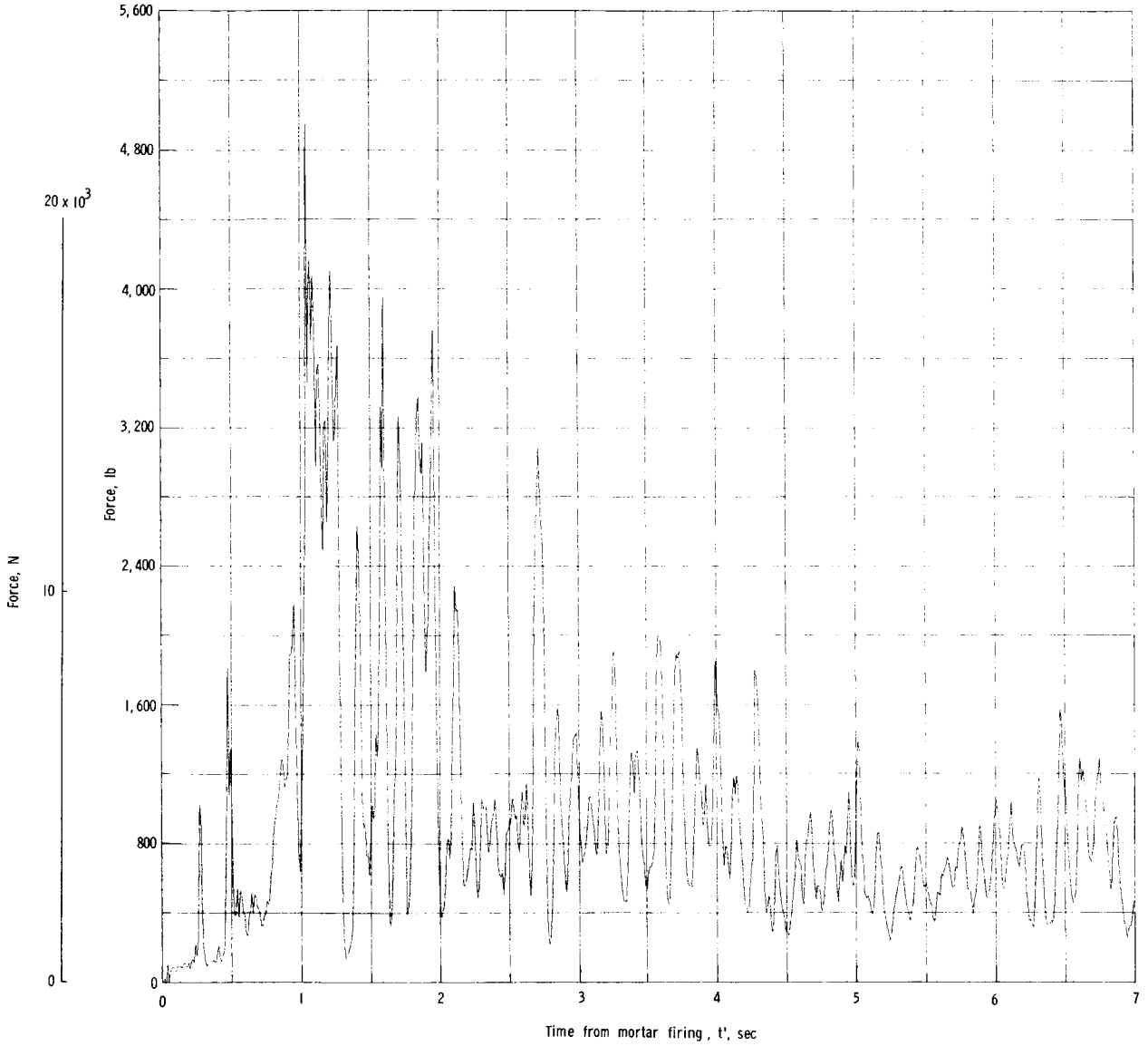

Figure 13.- Time history of force measured by the tensiometer.

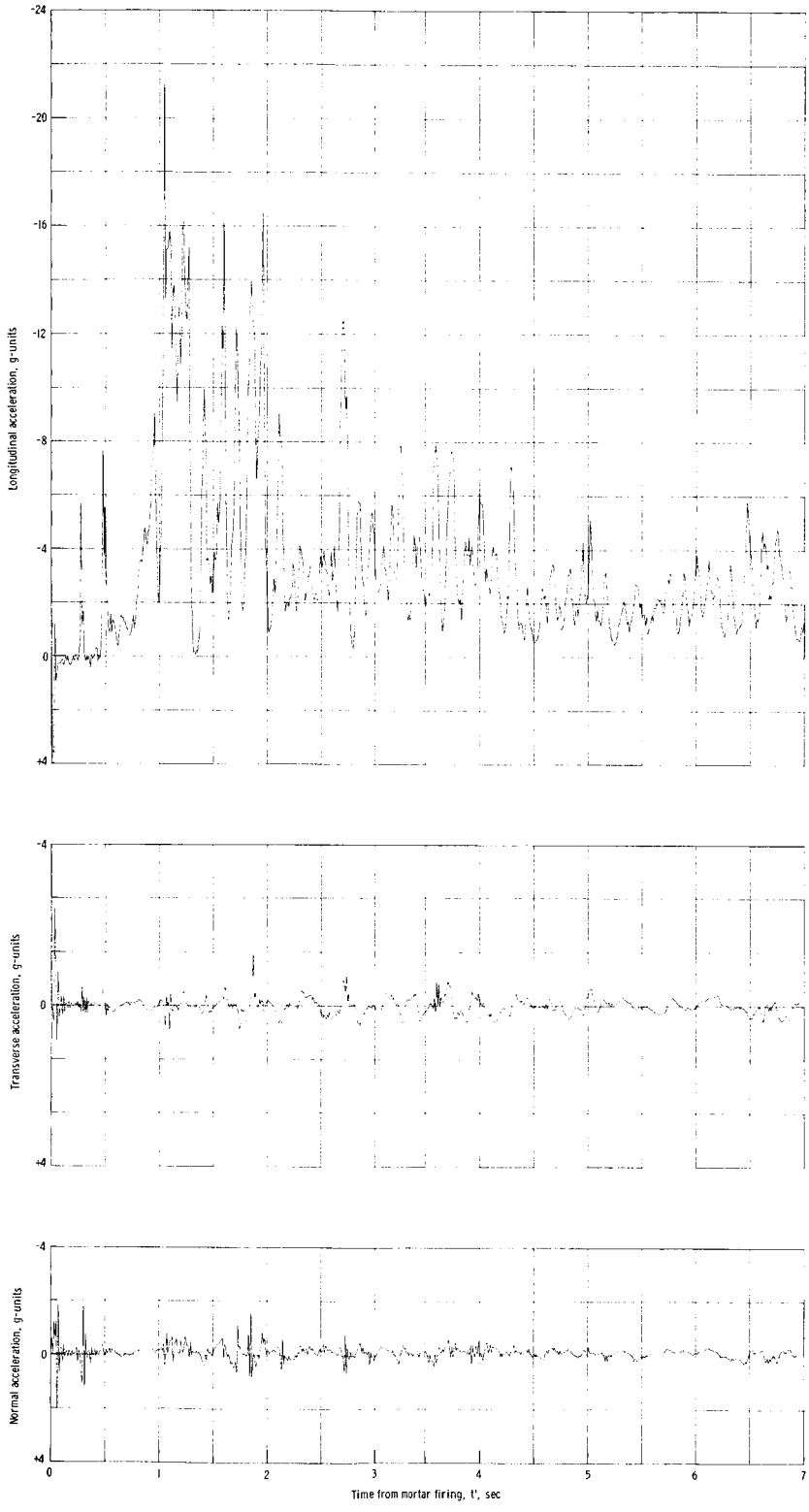

Figure 14.- Acceleration time histories.

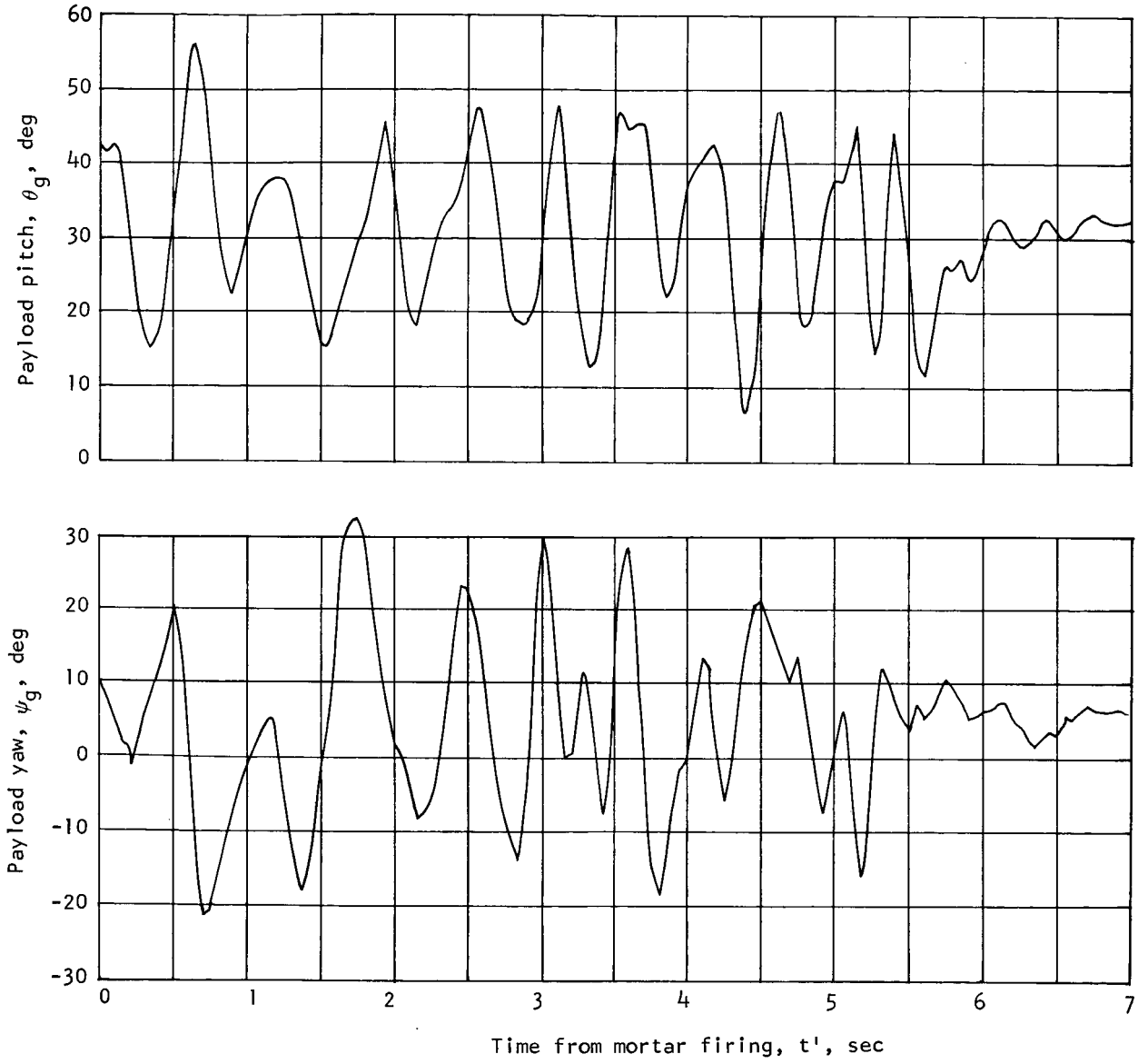

Figure 15.- Recorded payload pitch- and yaw-angle time histories.

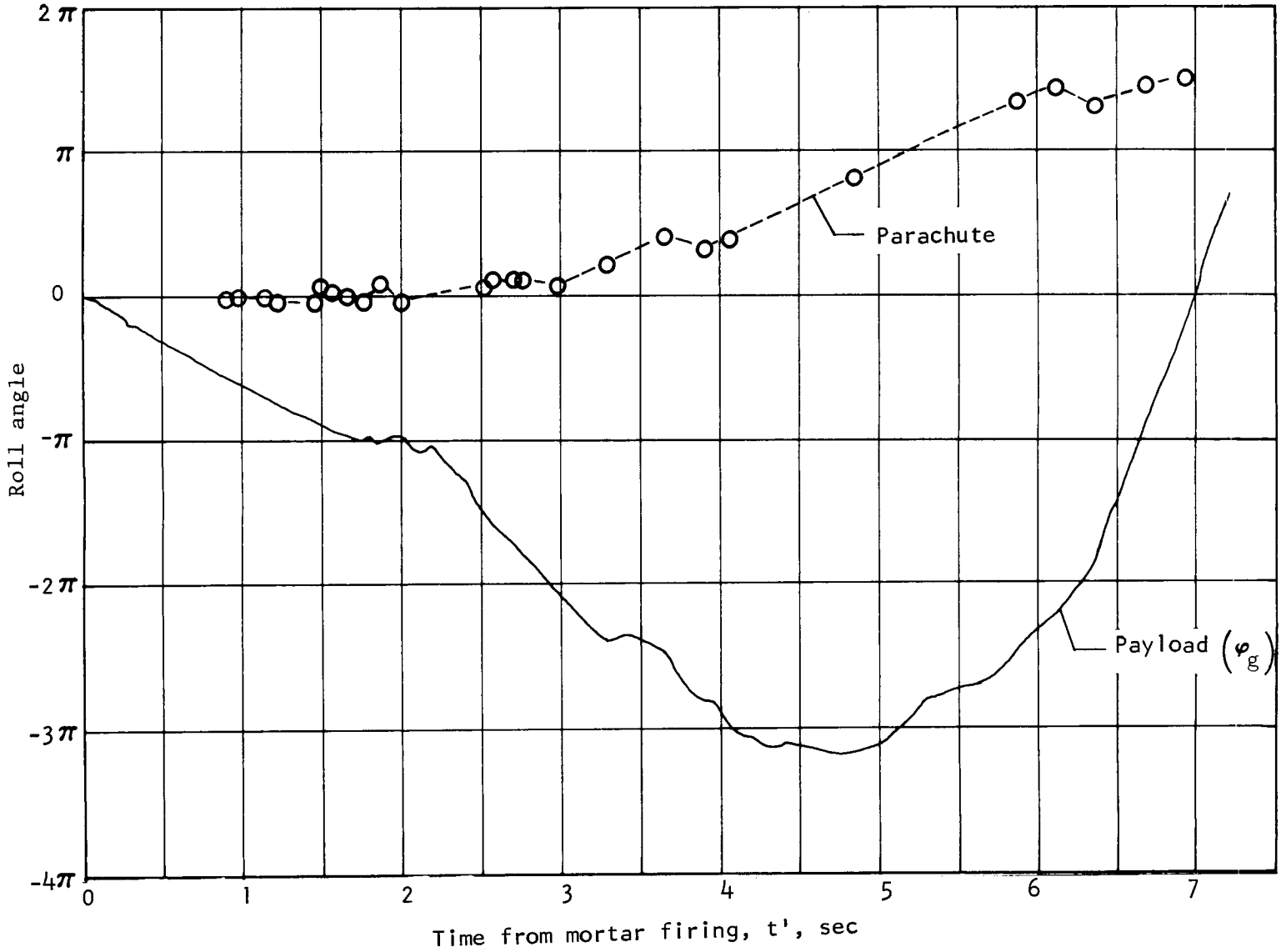

Figure 16.- Payload and parachute roll-angle histories.

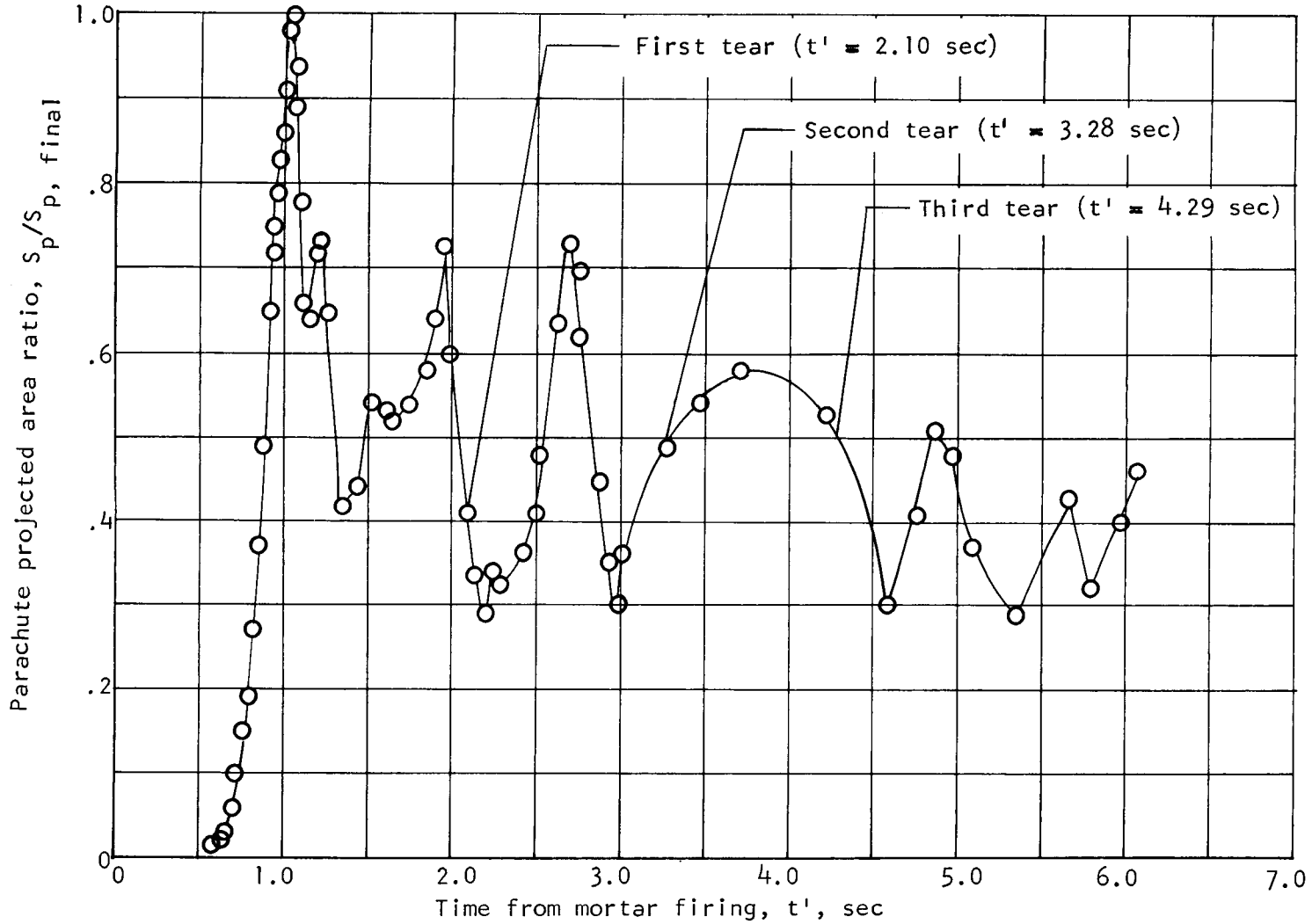

Figure 17.- Parachute projected-area-ratio time history.

t' = 0.48 second

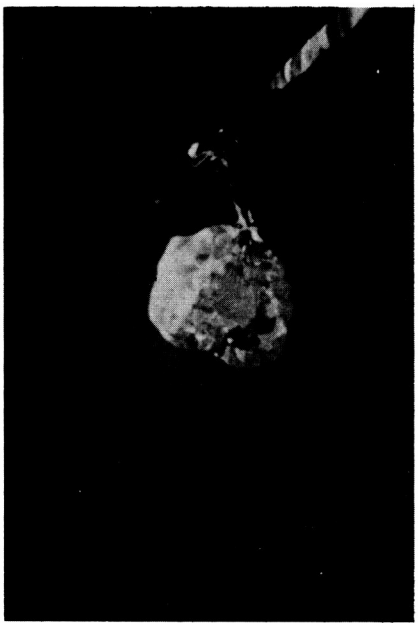

t' = 0.72 second

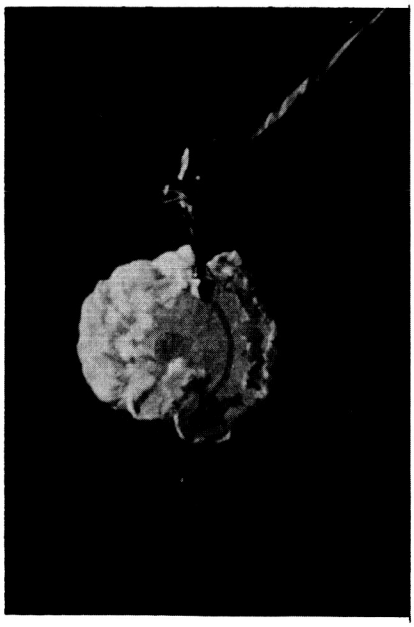

t' = 0.78 second

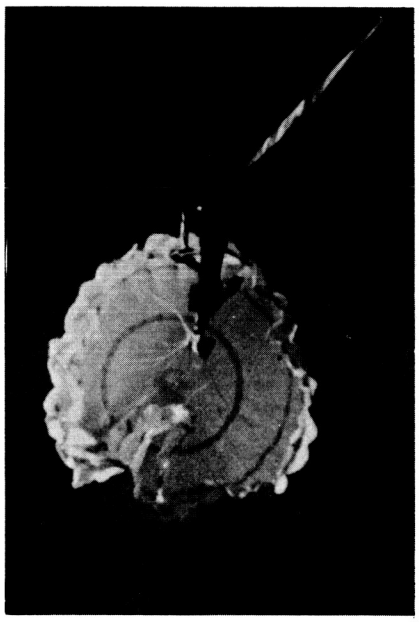

t' = 0.84 second

(a) Initial canopy inflation sequence. L-69-5115

Figure 18.- Onboard camera photographs.

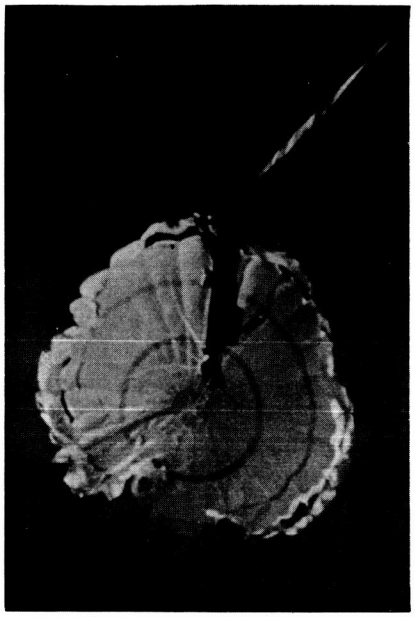

t' = 0.87 second

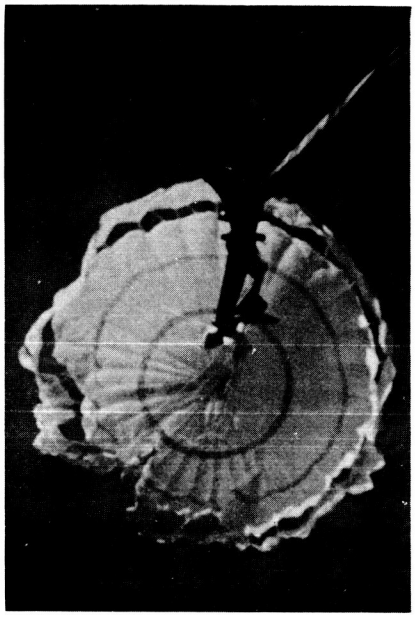

t' = 0.91 second

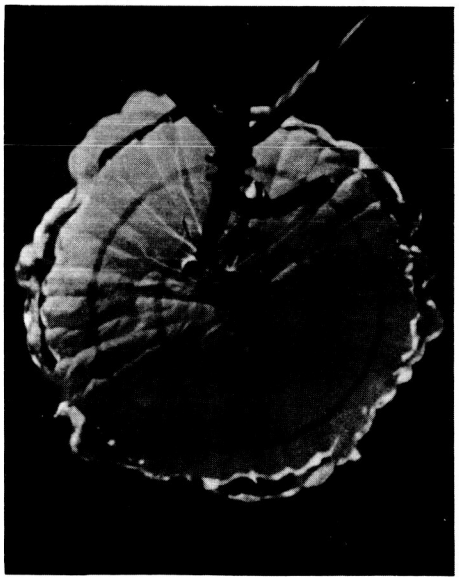

t' = 0.97 second

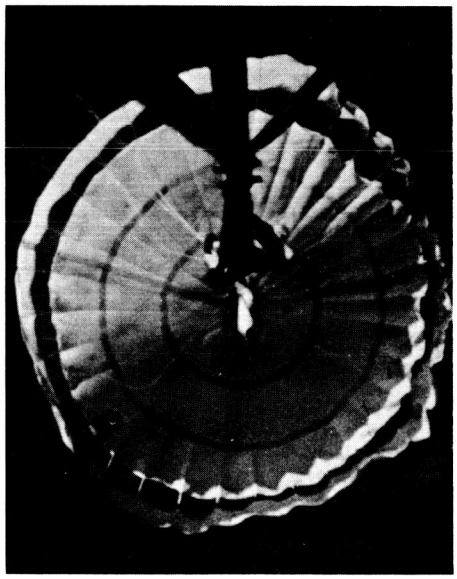

t' = 1.03 seconds

(a) Concluded.

L-69-5116

Figure 18.- Continued.

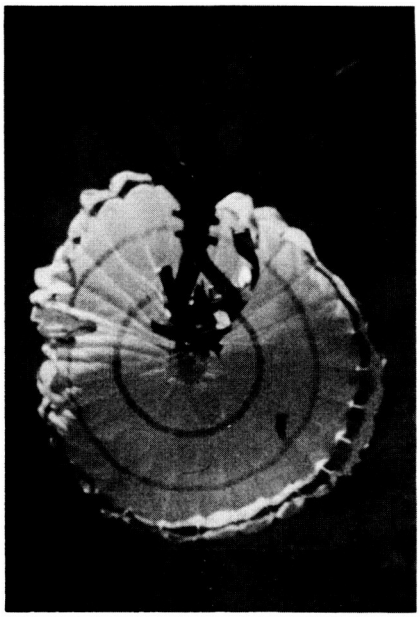

t' = 1.13 seconds

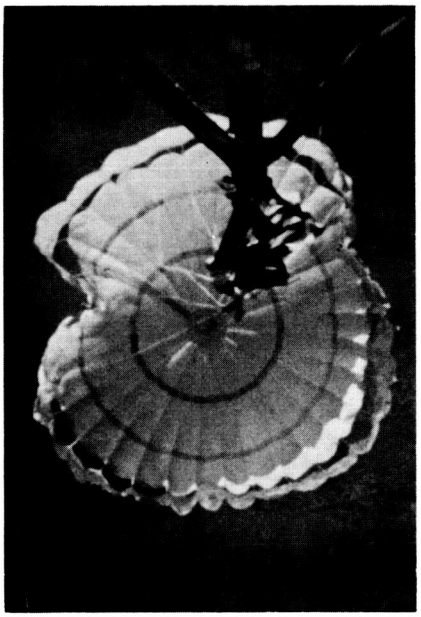

t' = 1.19 seconds

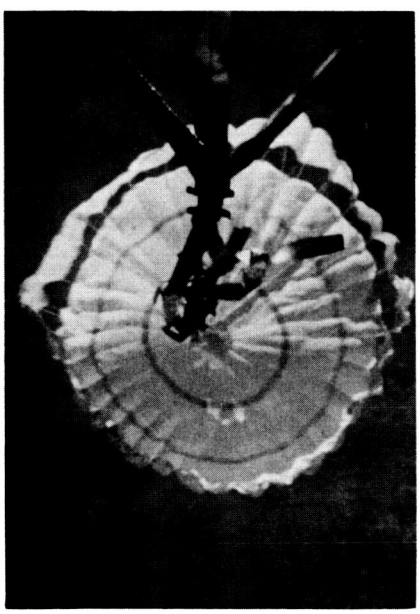

t' = 1.25 seconds

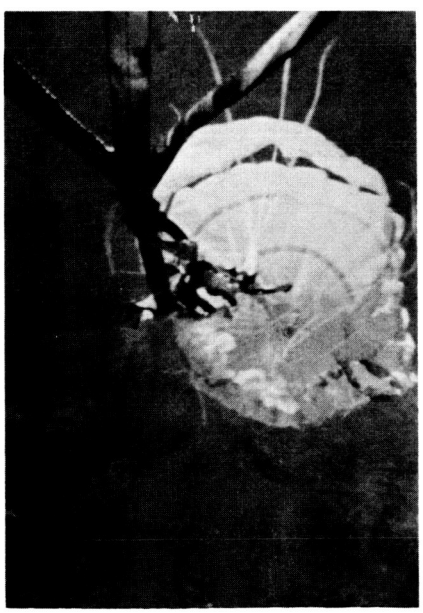

t' = 1.335 seconds

(b) Canopy collapse sequence. L-69-5117

Figure 18.- Continued.

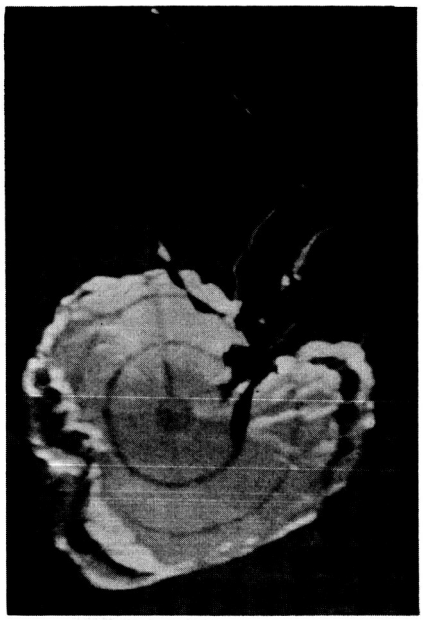

t' = 1.49 seconds
Tensiometer force,
618 lb (2 745 newtons)

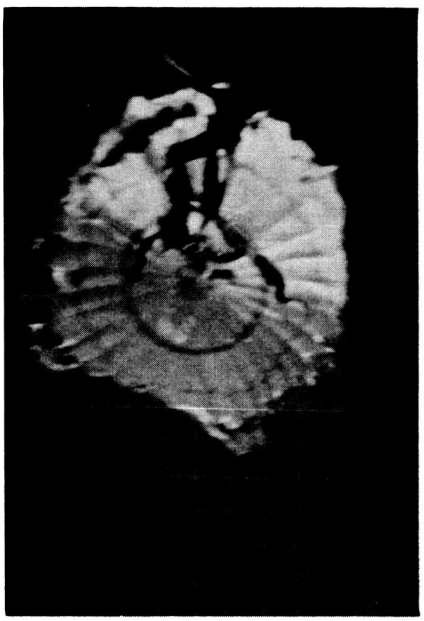

t' = 1.60 seconds
Tensiometer force,
3 950 lb (17 550 newtons)

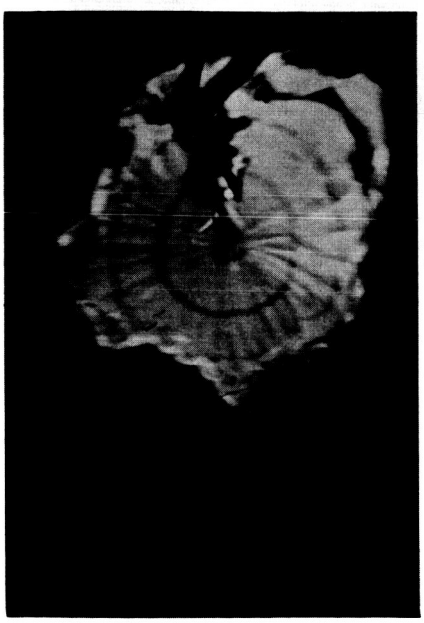

t' = 1.64 seconds
Tensiometer force,
323 lb (1 436 newtons)

t' = 1.71 seconds
Tensiometer force,
2 987 lb (13 295 newtons)

(c) Canopy load variation sequence. L-69-5118

Figure 18.- Continued.

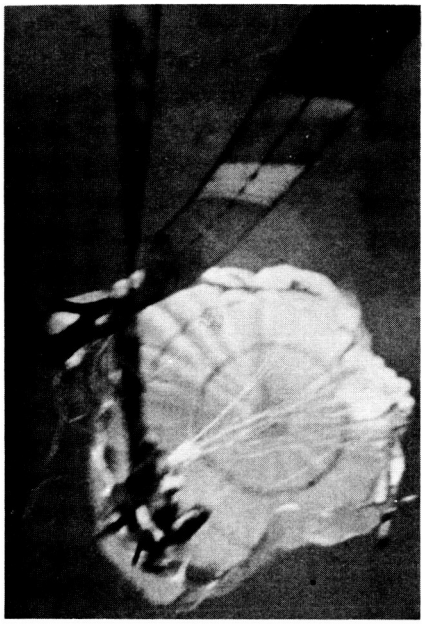

t' = 1.76 seconds
Tensiometer force,
390 lb (1 732 newtons)

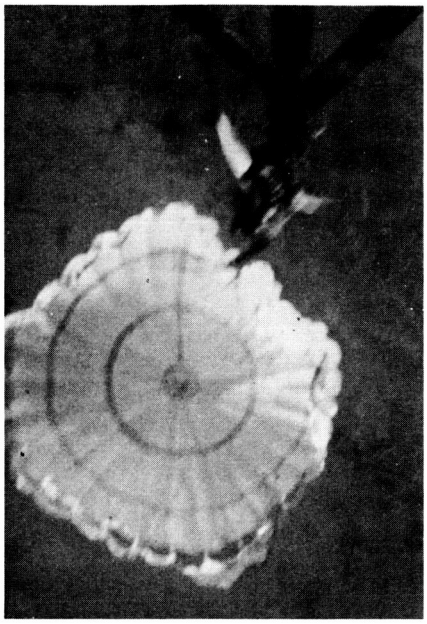

t' = 1.84 seconds
Tensiometer force,
3 282 lb (14 595 newtons)

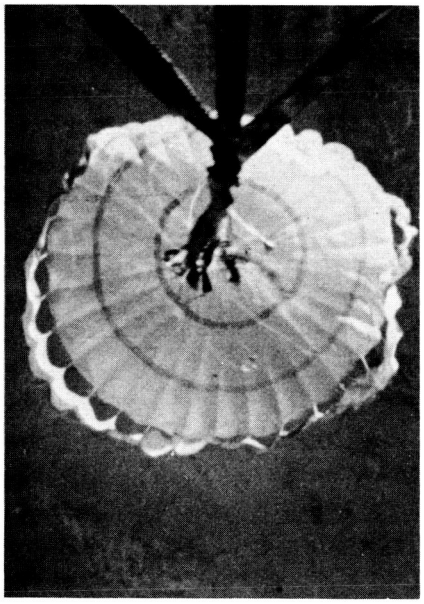

t' = 1.95 seconds
Tensiometer force,
3 762 lb (16 710 newtons)

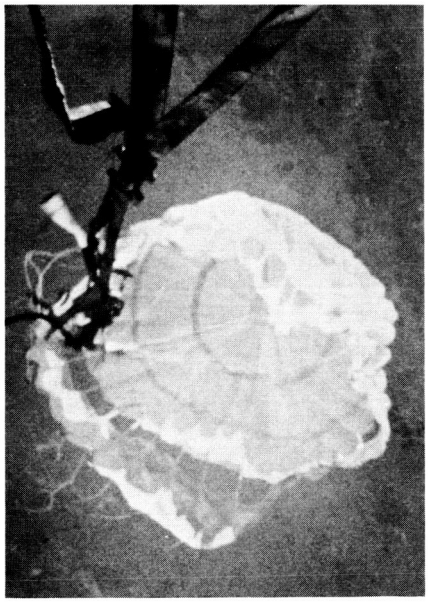

t' = 2.00 seconds
Tensiometer force,
446 lb (1 981 newtons)

(c) Concluded.

L-69-5119

Figure 18.- Continued.

t' = 2.10 seconds

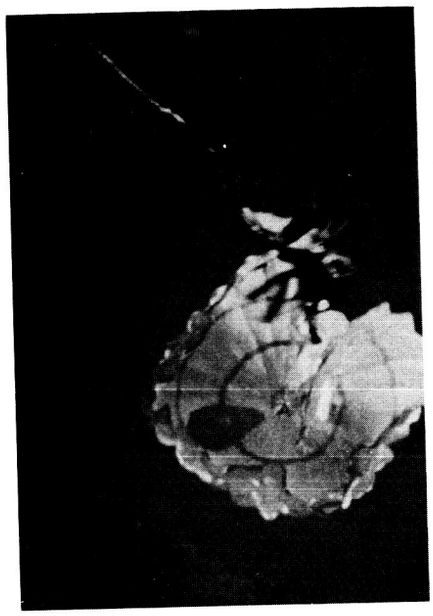

t' = 2.13 seconds

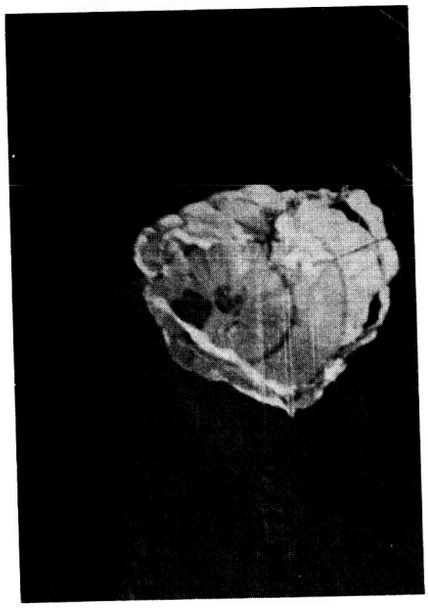

t' = 2.19 seconds

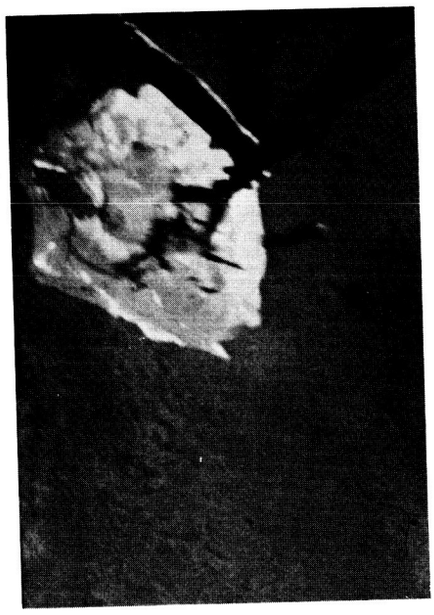

t' = 2.29 seconds

(d) Canopy damage sequence. L-69-5120

Figure 18.- Continued.

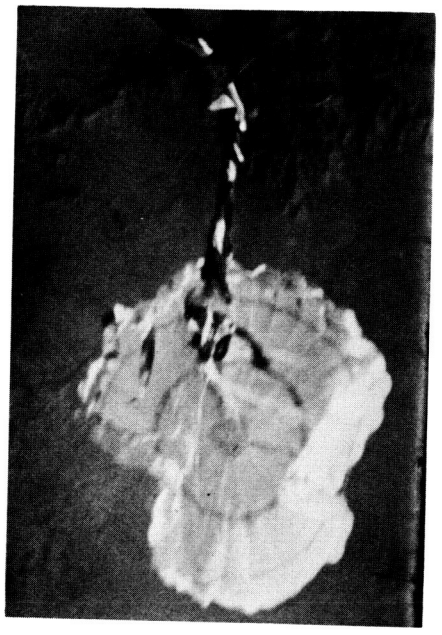

t' = 2.51 seconds

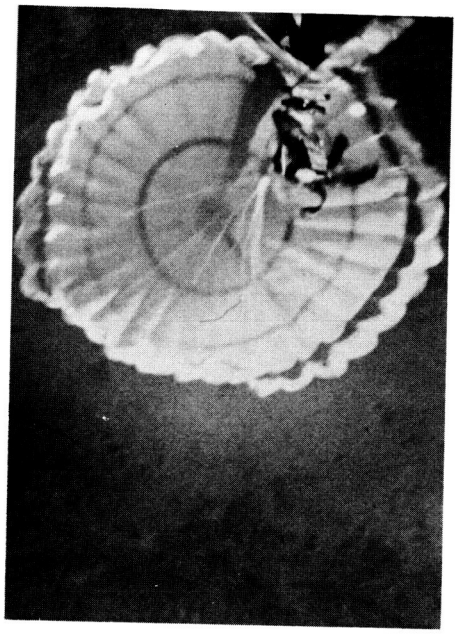

t' = 2.70 seconds

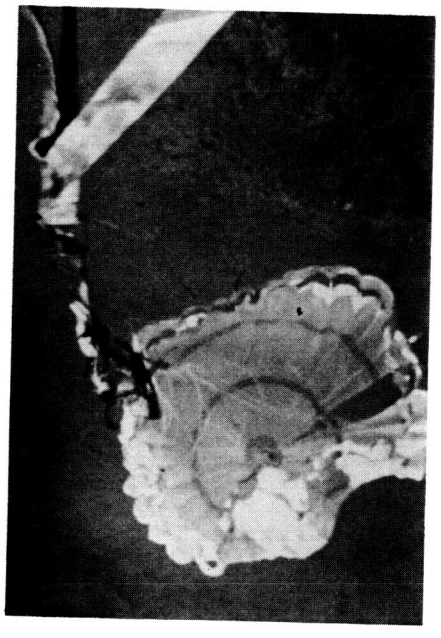

t' = 2.86 seconds

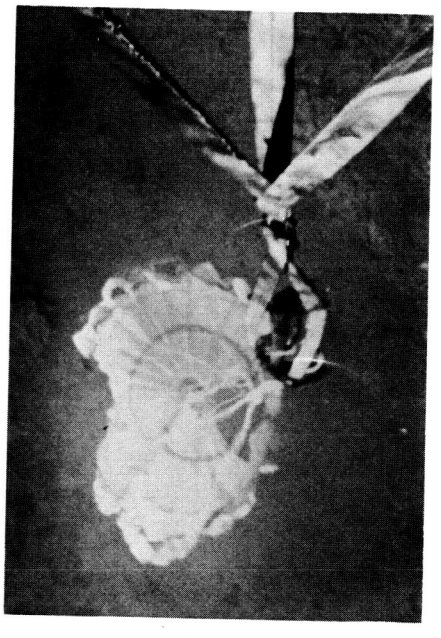

t' = 2.98 seconds

(d) Continued.

L-69-5121

Figure 18.- Continued.

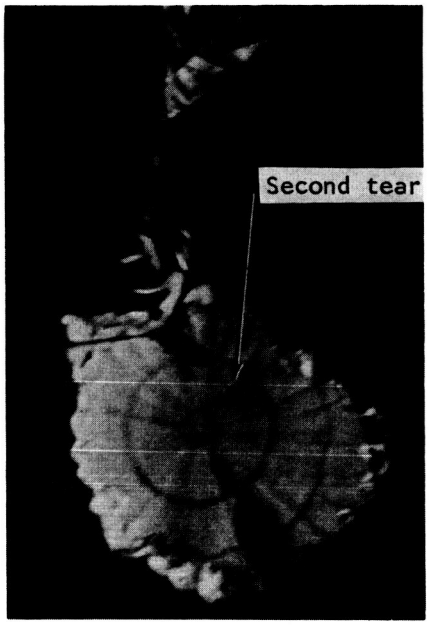

t' = 3.28 seconds

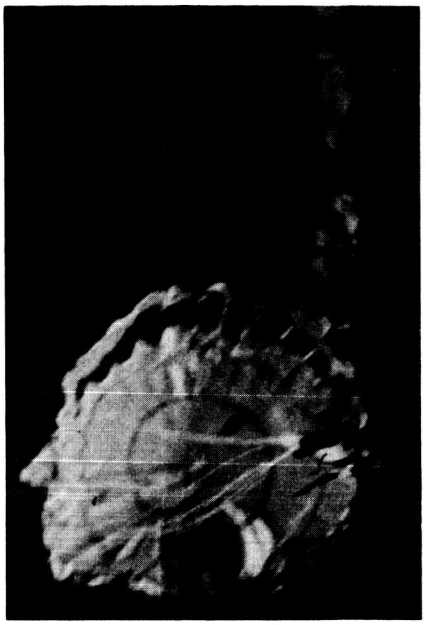

t' = 3.46 seconds

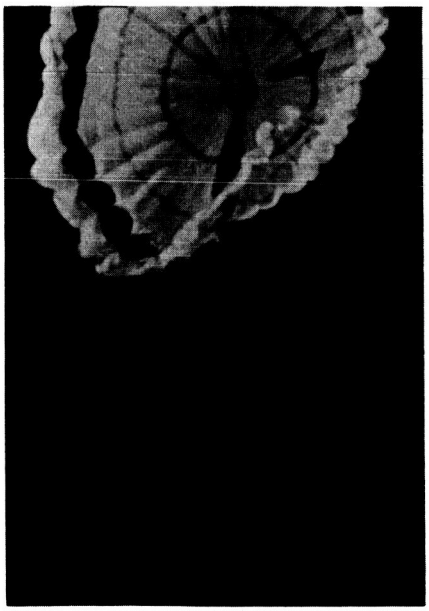

t' = 3.65 seconds

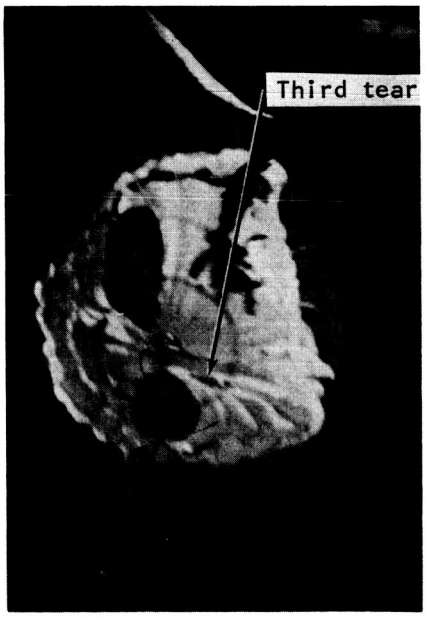

t' = 4.29 seconds

(d) Continued.

L-69-5122

Figure 18.- Continued.

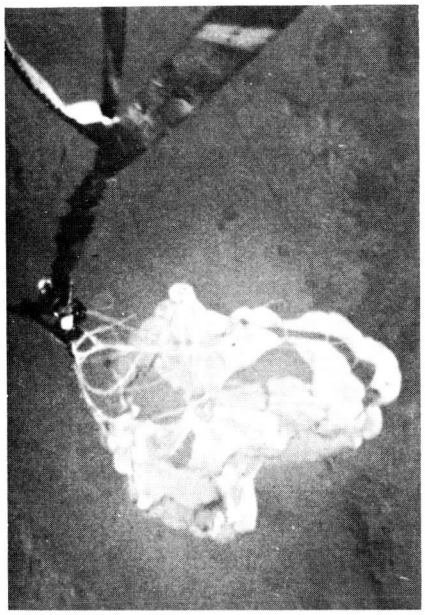

t' = 4.69 seconds

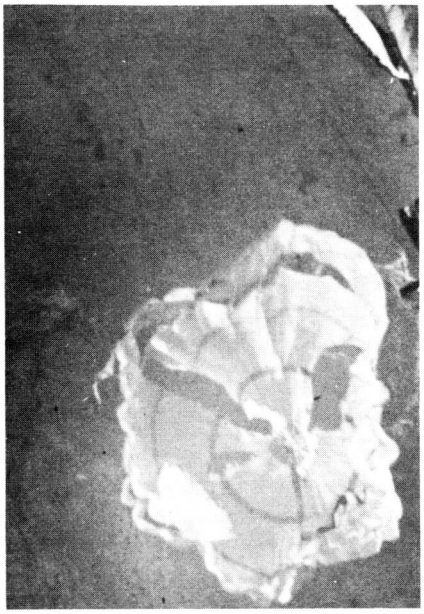

t' = 4.87 seconds

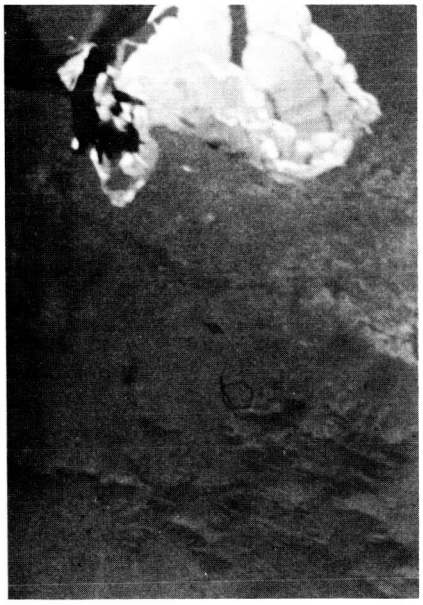

t' = 5.35 seconds

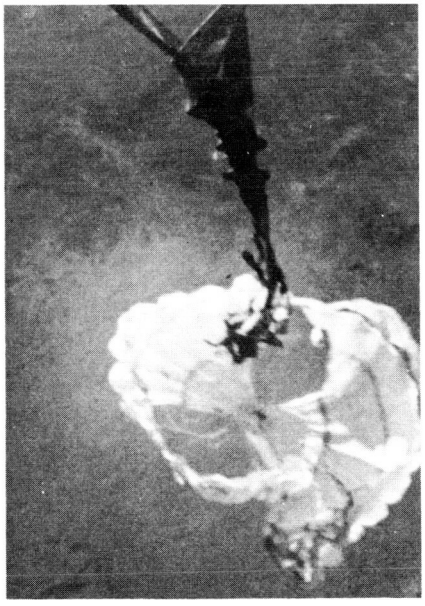

t' = 5.65 seconds

(d) Concluded.

L-69-5123

Figure 18.- Concluded.

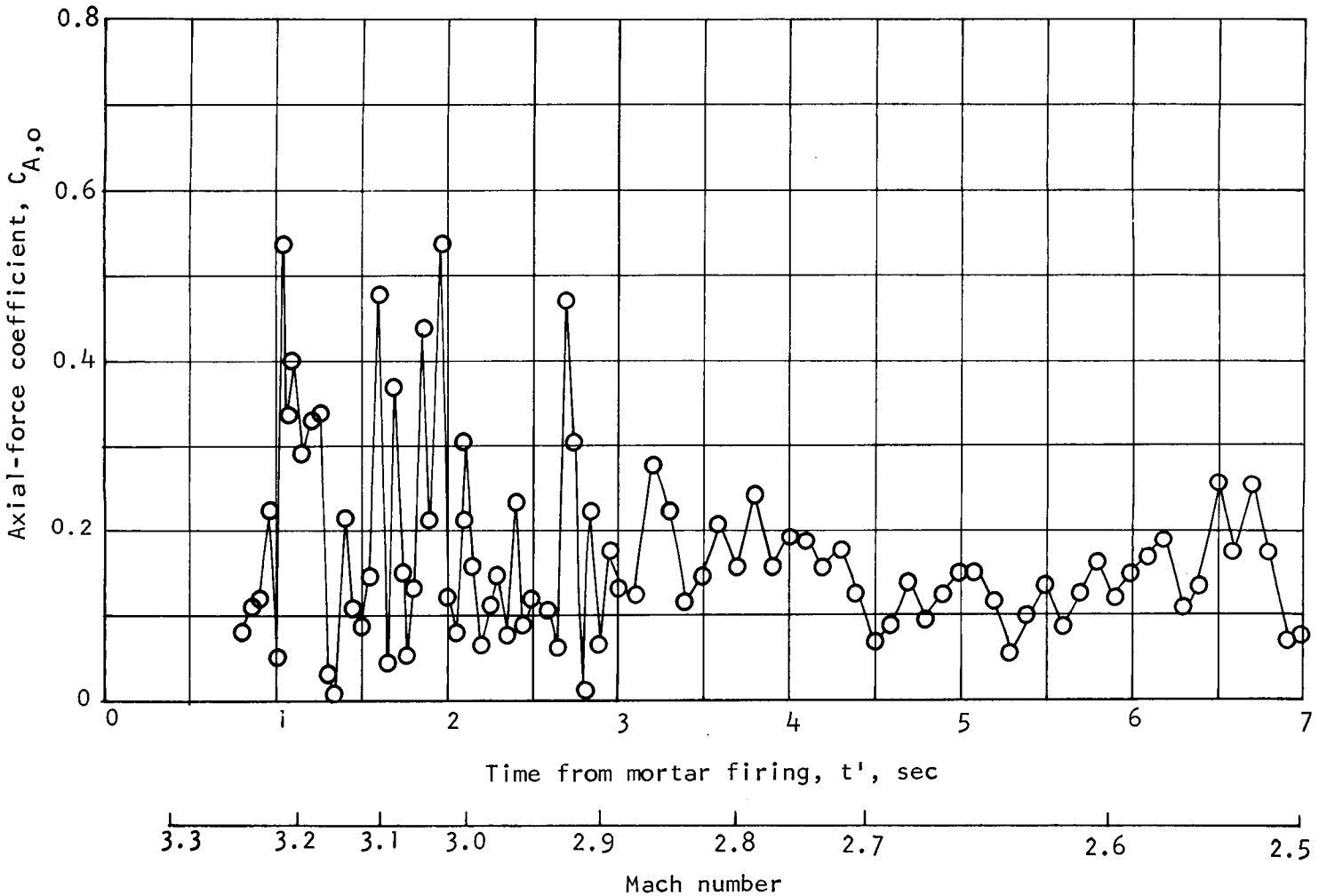

Figure 19.- Variation of nominal axial-force coefficient with time and Mach number.

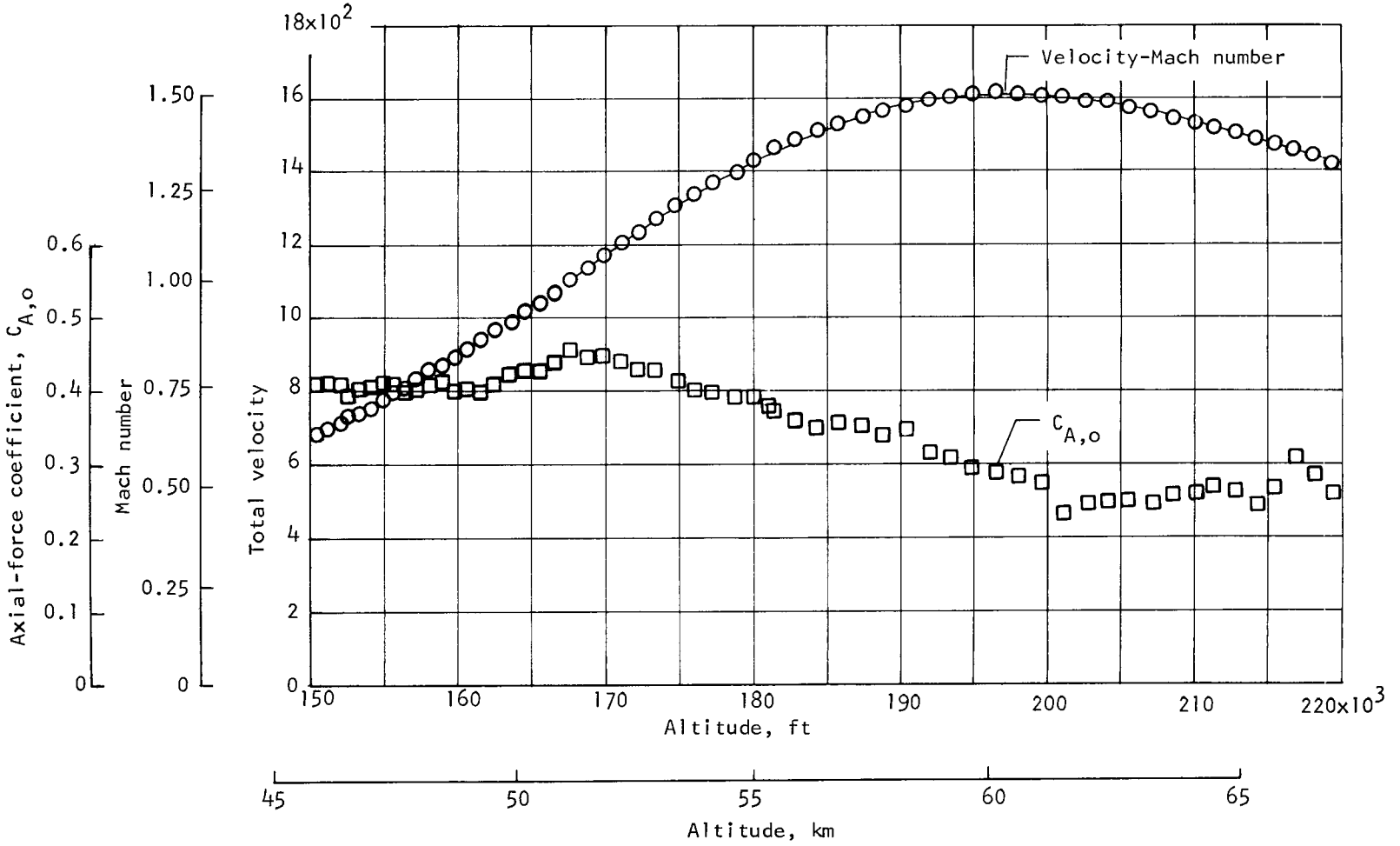

Figure 20.- Variation of total velocity, Mach number, and axial-force coefficient with altitude during descent above 150 000 feet (46 kilometers).

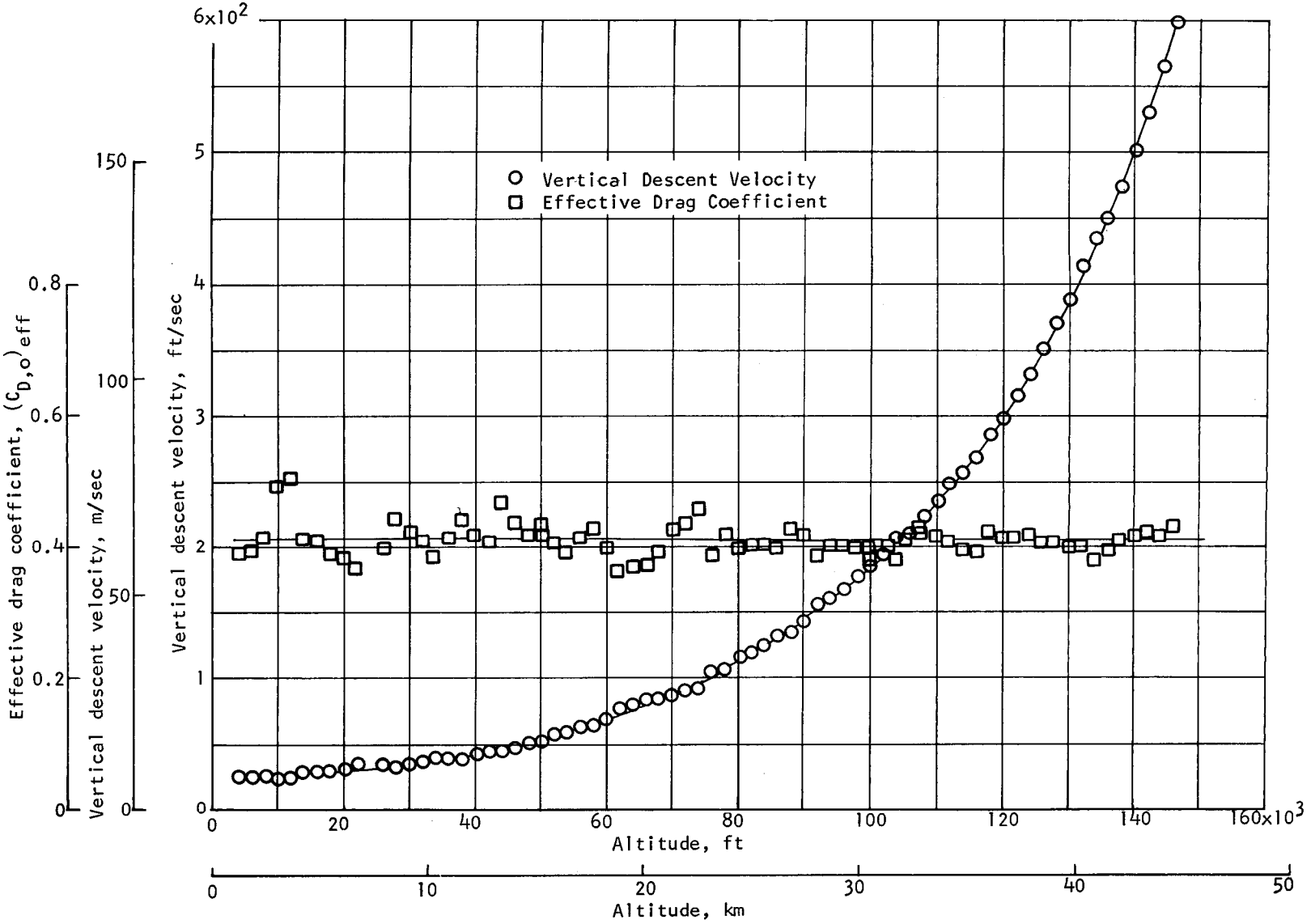

Figure 21.- Variation of vertical-descent velocity and effective drag coefficient with altitude.

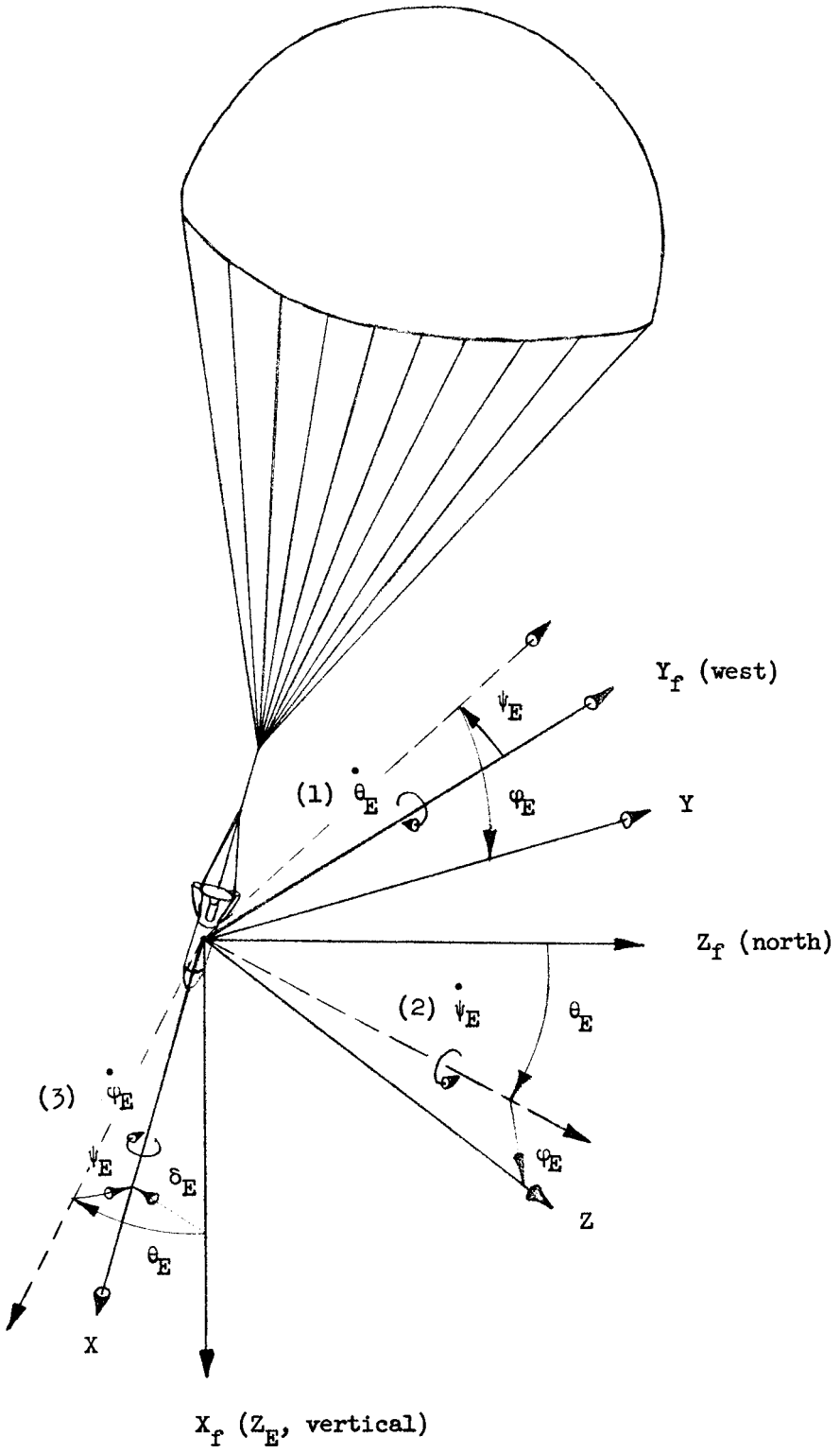

Figure 22.- Sketch showing relationship between body axes X,Y,Z and earth-fixed axes X_f, Y_f, Z_f.

Figure 23.- Time histories of pitch θ_E, yaw ψ_E, and the magnitude of the resultant angular displacement δ_E of the payload from the local vertical for a portion of descent from 137 000 to 100 000 feet (42 to 30 kilometers).

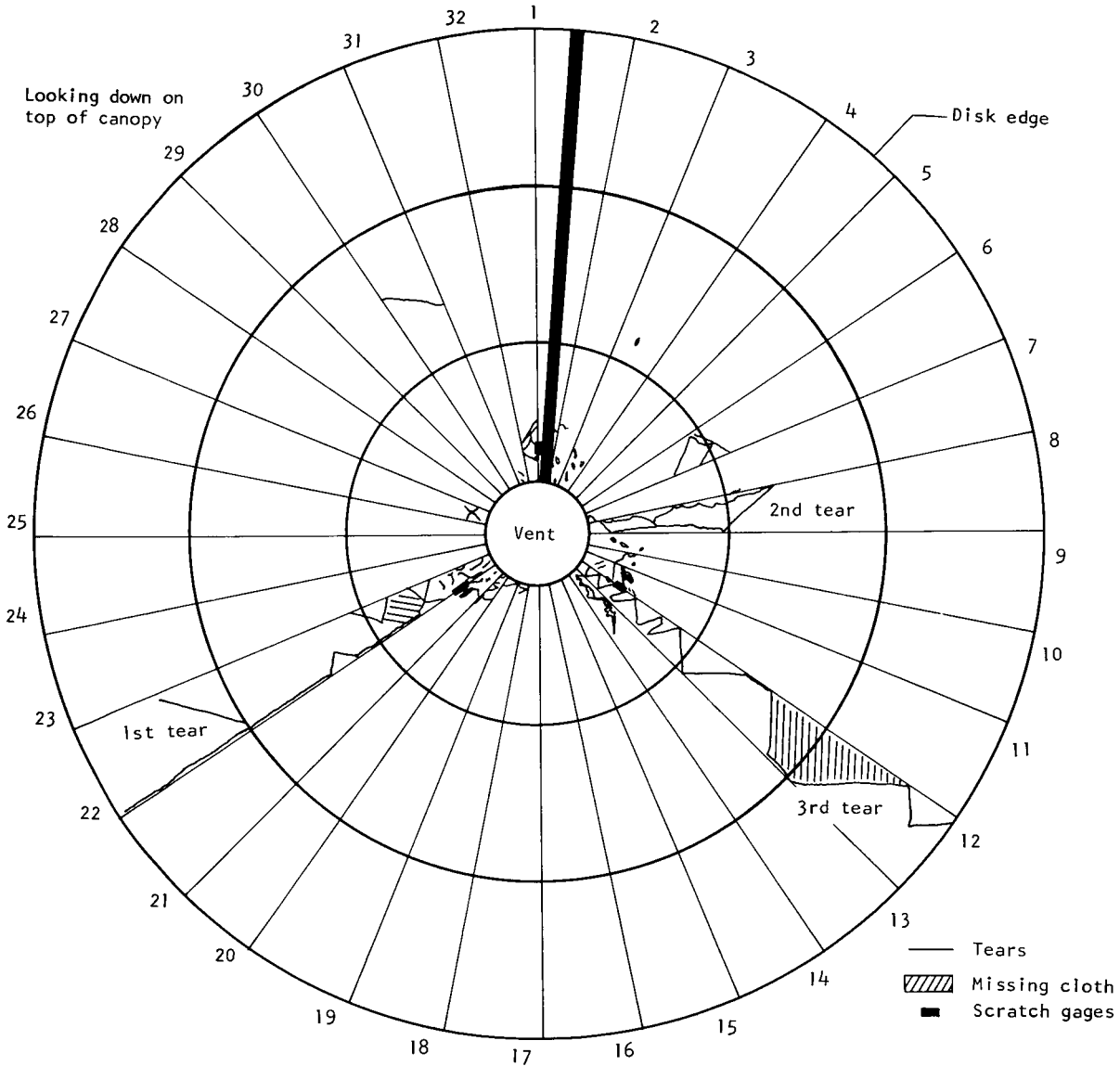

Figure 24.- Sketch showing damaged areas of the canopy.

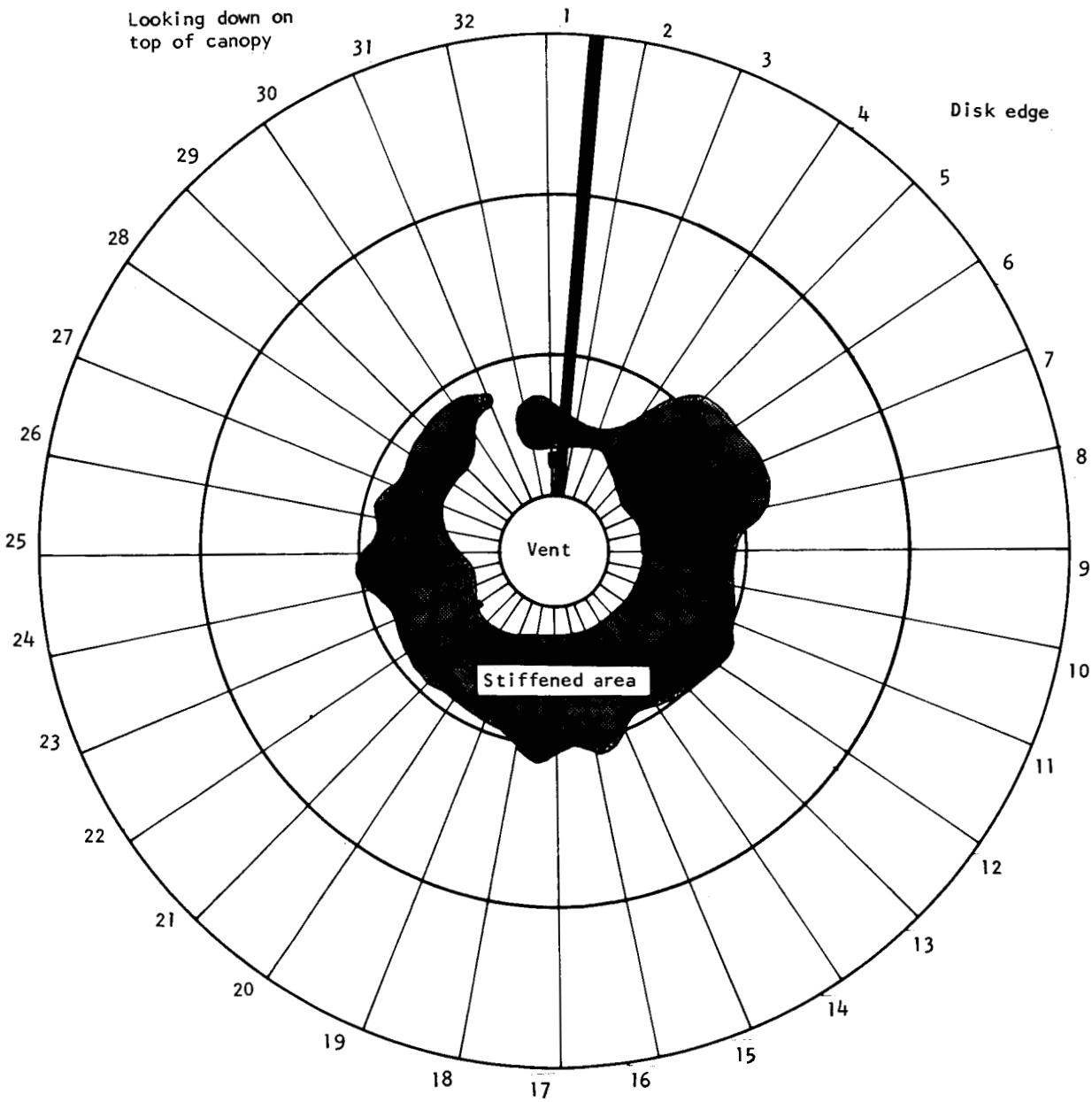

Figure 25.- Sketch showing stiffened area due to aerodynamic heating.